

Nanoscale

Accepted Manuscript



This is an *Accepted Manuscript*, which has been through the Royal Society of Chemistry peer review process and has been accepted for publication.

Accepted Manuscripts are published online shortly after acceptance, before technical editing, formatting and proof reading. Using this free service, authors can make their results available to the community, in citable form, before we publish the edited article. We will replace this *Accepted Manuscript* with the edited and formatted *Advance Article* as soon as it is available.

You can find more information about *Accepted Manuscripts* in the [Information for Authors](#).

Please note that technical editing may introduce minor changes to the text and/or graphics, which may alter content. The journal's standard [Terms & Conditions](#) and the [Ethical guidelines](#) still apply. In no event shall the Royal Society of Chemistry be held responsible for any errors or omissions in this *Accepted Manuscript* or any consequences arising from the use of any information it contains.



Nanoscale

REVIEW

Moving beyond flexible to stretchable conductive electrodes using metal nanowires and graphenes

Hanleem Lee^a, Ikjoon Kim^b, Meeree Kim^b and Hyoyoung Lee^{a,b*}

Received 00th January 20xx,
Accepted 00th January 20xx

DOI: 10.1039/x0xx00000x

www.rsc.org/

Stretchable and/or flexible electrodes and their associated electronic devices have attracted great interest because of their possible applications in high-end technologies such as lightweight, large area, wearable, and biointegrated devices. In particular, metal nanowires and graphene derivatives are chosen for electrodes because they show low resistance and high mechanical stability. Here, we review stretchable and flexible soft electrodes by discussing in depth the intrinsic properties of metal NWs and graphenes that are driven by their dimensionality. We investigate these properties with respect to electronics, optics, and mechanics from a chemistry perspective and discuss currently unsolved issues, such as how to maintain high conductivity and simultaneous high mechanical stability. Possible applications of stretchable and/or flexible electrodes using these nanodimensional materials are summarized at the end of this review.

1. Introduction

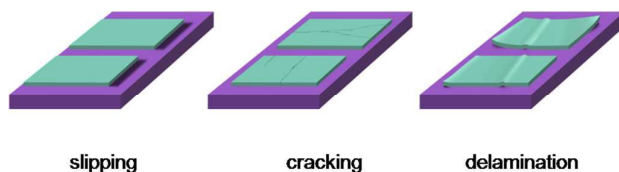


Fig. 1 Three classes of possible failure mode for stretchable and flexible electronics.

In recent years, stretchable or flexible types of robotic skins¹, morphing touch screens², biometric devices³, wearable supercapacitors⁴, and solar cells⁵ have been successfully produced. Stretchable and/or flexible electronics are commonly fabricated on polymer substrates such as polyethylene terephthalate (PET), polyethylenimine (PEI), or polydimethyl-siloxane (PDMS) rather than a rigid substrate. The elastic nature of the substrate effectively suppresses strain localization on the relatively rigid active layer, leading to the realization of bendable, stretchable, and three-dimensional (3D) attachable devices (wearable displays, therapeutic biointegrated devices, and real-time healthcare monitoring). Stretchable and/or flexible electronics can be categorized into microelectronics and flexible electronics. In microelectronics, hard unit devices link with flexible interconnectors. Most of

the strain stress is accumulated on a flexible conductive interconnector and the rigid microelectronic unit device on the polymer substrate survives during bending/stretching. Metals with new structural layouts serve as interconnectors. The thickness of the conductive material influences the ductility of film such that bending strain decreases linearly with thickness⁶. Very thin metal can sustain a large strain and avoid subsequent deformation; however, it is not sufficient for the generation of completely stretchable or flexible electrodes due to defects⁷, elastic mismatch between substrate and conductive materials⁸, weak adhesion⁹, and the size of the hard unit device^{10,11}. Additional 2D or 3D layout structure can facilitate mechanical stability during operation: a wavy structure using mechanical buckling¹², a 2D horseshoe configuration¹³, percolation network¹⁴, and 3D configurations such as mesh layouts with planar leaf-arm¹⁵, coiled springs¹⁶, and non coplanar configurations¹⁷. The curvature of shape and the degree of percolation govern the strength of a material, which is the ability to withstand an applied stress without failure^{18,19}. Figure 1 shows three failure modes of cracking/channelling, sliding, and delamination (or debonding). They are dominant in new structural layouts strategy and the interfacial state between the polymer and conductive film determines the type of failure²⁰. Cracking occurs under tensile strain or in a strongly adhered film, whereas channelling occurs under compressive strain or in a weakly adhered film. However, in spite of the remarkable stretchability and flexibility of electrodes with the new structural layout, the complicated fabrication and low transparency hinder integration of these optoelectronic devices over a large area.

^a Center for Integrated Nanostructure Physics, Institute for Basic Science (IBS), and Department of Energy Science, Sungkyunkwan University, Suwon 440-746, Korea

^b Department of Chemistry, Sungkyunkwan University, Suwon 440-746, Korea

† Footnotes relating to the title and/or authors should appear here.

Electronic Supplementary Information (ESI) available: [details of any supplementary information available should be included here]. See DOI: 10.1039/x0xx00000x

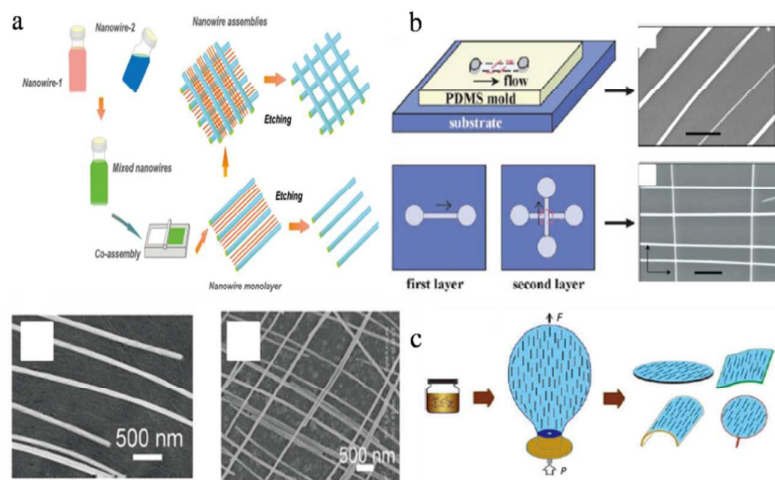


Fig. 2 Representative coating method for ordered morphology. Schematic illustrations of a) NW co-assembly process⁵⁹, b) Parallel array of NW by microfluidic method³⁵, and c) blown bubble film process³⁷.

Another strategy to achieve a soft electrode is the use of new materials. Conductive polymers, graphene, carbon nanotubes (CNT), and metal nanowires (NW) have been intensively studied not only as conductors, but also as transparent conductive films in soft electronics. New materials have been widely used to overcome several unsolved challenges for conventional soft electronics: (1) Stable device performance under conditions of high strain and omni-direction, (2) High-quality electronic performance with excellent mechanical robustness, (3) High interfacial interaction with the human body in the case of bio-integrated devices, (4) Simple fabrication method, and (5) The need for high transmittance with high conductivity for optoelectronics. Especially, graphene and metal NWs have been considered as candidates to substitute for indium tin oxide (ITO) or rigid metal film in soft electronics. Both graphene and metal NW can be flexible in a certain direction as a result of their ultrathin nature, but their stretchability relies on the dimensionality. Only 1D NW exhibits high stretchability through the design of a percolating network whereas it is hard to make 2D graphene stretchable. For stretchable electronics with graphene, a new structure layout strategy and percolation network with reduced graphene oxide (rGO) has been suggested. Kim et al. report that graphene films show mechanical failure beyond ~6% on the unstrained PDMS substrate, compared with 12% on the prestrained PDMS substrate²¹. In addition, in the case of an Ag nanowire (AgNW), the biggest problem associated with this strategy is the high resistance changes for initial elongation compared with that of metallic materials with a new structure layout.

Here, we review stretchable and flexible soft electrodes generated using metal NWs and graphene derivatives of great interest, and also introduce their unique properties and possible applications. Several excellent reviews on the trend of stretchable and flexible electronics have been published recently, mainly dealing with layout strategy^{22,23}. Regarding new materials for the soft electrode, however, most reviews

only provide a brief introduction about materials processing techniques and flexible electrodes, with very limited information on stretchable electrodes despite the huge interest in this area. Therefore, in this review we aim to discuss in depth the intrinsic properties of new electrode materials and methods to control their properties, allowing us to evaluate the benefits of stretchable electrodes over flexible electrodes. To avoid an immense volume of information, we will focus only on metal NW and graphene, which show high conductivity and high mechanical stability, among other known candidates. First, we will introduce the properties of metal NW and graphene that are driven by their dimensionality and discuss unsolved issues for each material. Second, the strategy for enhancing electrical and mechanical properties with NW and graphene will be covered from

the perspective of chemistry. Possible applications of the stretchable electrodes instead of or with flexible electrodes using these nanodimensional materials are summarized at the end of this review.

2. Soft electrode materials

There are many conductive materials such as metals, conductive polymers, carbon allotropes, and conductive nanocomposites. In recent studies, a nanostructure of these conductive materials has been widely used due to the extraordinary electrical and/or mechanical properties driven by their dimensionality. In this chapter, we will discuss in depth the intrinsic properties of metal NW and graphene in terms of dimensionality and also introduce processing techniques and associated issues.

2.1. One-dimensional metal NW

2.1.1. Percolation theory. 1D nanostructures such as nanowires, nanorods, nanotubes, and nanobelts are good candidates for both interconnects and functional units in soft electronics, soft optoelectronics, and soft electrochemical devices because the 1D material exhibits a strong tolerance to stretching as a result of intersliding behaviour. The percolation theory plays an important role in determining electrical, optical, and mechanical properties of 1D materials. The percolation theory for 1D wires approximately predicts a threshold areal wire density (N_c) by equation 1 and sheet resistance of network by equation 2²⁴. The resistance of the network is related to NW length, density, and NW diameter.

$$\begin{aligned} 1) \quad & L_s \sqrt{\pi N_c} = 4.236 \\ 2) \quad & R_s \propto (D - N_c)^\alpha L_s^\beta \end{aligned}$$

Where L_s is the average NW length, D is density of the NW, α is a parameter related to spatial arrangement, and β is a parameter related to junction resistance and intrinsic conductivity of the material. A network with longer NW with small diameter and higher density shows a lower resistance

because of its percolative nature. However, a network with very small diameter presents higher resistance because the mean free path of electrons of the bulk materials is smaller due to surface scattering of the electrons, which is dominant over the percolation theory. In addition, the alignment of NW also attributes to the resistance of network. When the number of junctions between NWs is large and/or the degree of contact length is small, the network resistance increases. Vigolo et al. found that a single wall CNT (SWNT), which is another example of 1D material in an aqueous surfactant solution, leads to higher percolation thresholds than the SWNT without surfactant²⁵. The surfactant prevents intermolecular interaction between SWNTs, whereas SWNTs without surfactant adhere strongly by van der Waals force interactions, resulting in an increase in the effective length of SWNTs network. The alignment of the NW network affects not only the electrical property, but also various unique properties because of the dramatic increase in surface area/volume ratio and the manifestation of collective nanoscale properties. Optical property change is the best-known phenomenon. The optical features of a 1D material are dominantly caused by quantum confinement effects, such that a different optical signature occurs depending on the growth direction of NW. Another significant character of the metal NW is two surface plasmon resonance modes (SPR, transverse mode and longitudinal excitation). These two SPRs show a different tendency; the wavelength of the transverse mode is fixed depending on the type of metal (approximately 410 nm for Ag), whereas their longitudinal modes are fixed or broadened by distribution of the aspect ratio and their morphology²⁶. Hong-Yan Shi et al. demonstrated that the degree of change in electromagnetic fields is related to the ordering of the NW²⁷. The electromagnetic field coupling between the aligned NW shows peak broadening in the 700-800 nm range and the transmission intensity changes depending on the polarization angle, whereas the randomly deposited NW does not show these effects. The other interesting feature is that NW shows higher transmittance than bulk material. The vacancy of the network plays an important role in transparency because the transmittance loss is mainly induced by reflective scattering of light by the 1D shape of NWs.

Table 1. Coating method

Ordered shape	Disordered shape
Langmuir-Blodgett(LB) ^{28,29}	Spray coating(air brush ⁴³ , electro hydro-dynamic method ⁴⁴ , electrostatic method ⁴⁵) Vacuum filtration ⁴⁶ Rod coating ⁴⁷ Drop casting ^{48,49,50} Spin coating ⁵¹ Solvent evaporation method(vertical spinning ⁵²) Slot-die coating ⁵³ Doctor blade coating ⁵⁴ Controlled dip coating ⁵⁵ Layer-by-layer assembly ⁵⁶
Evaporation induced assembly ³⁰	
Mechanical force	
(contact printing method ³¹ , roll printing method ^{28,32})	
Strain release assembly ³³	
External nanostructure	
(coassembly behavior ⁵⁹)	
Microfluidic flow ^{34,35}	
Bubble-blowing process ³⁷	
Magnetic field, electric field ³⁹	
Electrophoresis ⁴⁰	
Electrospinning ⁴¹	
The knocking down method ⁴²	

In fact, the haze factor, which is the degree of scattering of transmitted light, becomes a more critical factor. The haze can be controlled by NW density, diameter, coating method, and post processing. Lower diameter and longer length of NWs lead to a larger vacancy, minimizing the light scattering. Thus, the degree of vacancy is strongly dependent on the fabrication method. To obtain the desired properties, many researchers have tried to engineer well-defined ordered complex architectures. These findings are summarized in Table 1.

2.1.2. Coating Method. Coating methods for the flexible electrode can be divided into two categories: the first is to make an ordered network and the second is to make a disordered network. The well-ordered network can be fabricated by interface-induced assembly^{28,29}, external field-induced assembly^{38,39}, microfluidic flow³⁵, bubble-blowing process³⁷, and electrospinning⁴¹. The Langmuir-Blodgett (LB) technique is a representative coating method using an interface-induced assembly. Tao et al. produced a densely packed AgNW layer by the LB method for high-performance electronics⁵⁷. AgNWs with thiol ligand are spread onto a water-supported surface. Ligand exchange from the PVP capping agents to the thiol ligand is crucial to alter the NW hydrophobic surface. After evaporation of the volatile solvent, the sample is compressed slowly. As a result, an AgNW network forms an isotropic phase assembled film because of both material-material and material-substrate interactions⁵⁸. The alignment depends on the nanomaterial's size distribution and dewetting of the solvent during the assembly process. Others suggested a co-assembly of two NWs using the LB method to synthesise a uniform mesh like a network(Figure 2a)⁵⁹. They demonstrated an AgNW and TeNW co-assembly network using the LB method, followed by etching of TeNW by treatment with 1 M NaOH solution at room temperature. The molar ratio of two NWs can determine the vacancy of the network. Microfluidic flow is another famous coating method because NW strongly follows the rheological behaviour of solution. The NW network with a mesh-like assembly using a fluidic alignment with surface patterning techniques is presented in Figure 2b³⁵. The parameters affecting alignment are flow time, flow rate related to shear force, and concentration of NW. The combined effect of the capillary flow and strong interaction makes NWs ordered. In addition, Yu et al. report a blown bubble method that can fabricate a network with NW on a large wafer(Figure 2c)³⁷. A homogeneous concentration polymer suspension of NWs is expanded using a circular die to form a bubble and then the bubble film is transferred to the substrate. Pressure, external vertical force, and concentration of NW are modulated to control the alignment of film. Even though it is much easier to manipulate the desired property of ordered NW, most methods are complex and it is hard to make a film with a large area. To solve this problem, new types of coating method were developed: Meyer rod coating⁴⁷, drop casting⁴⁸, spin coating⁵¹, spray coating⁴³, layer-by-layer assembly (LBL)⁵⁶, vacuum filtration⁴⁶, and solvent evaporation⁵². A disordered NW with a certain degree of uniformity is produced by these methods. In the case of Meyer rod coating, a rod with wire coils is used.

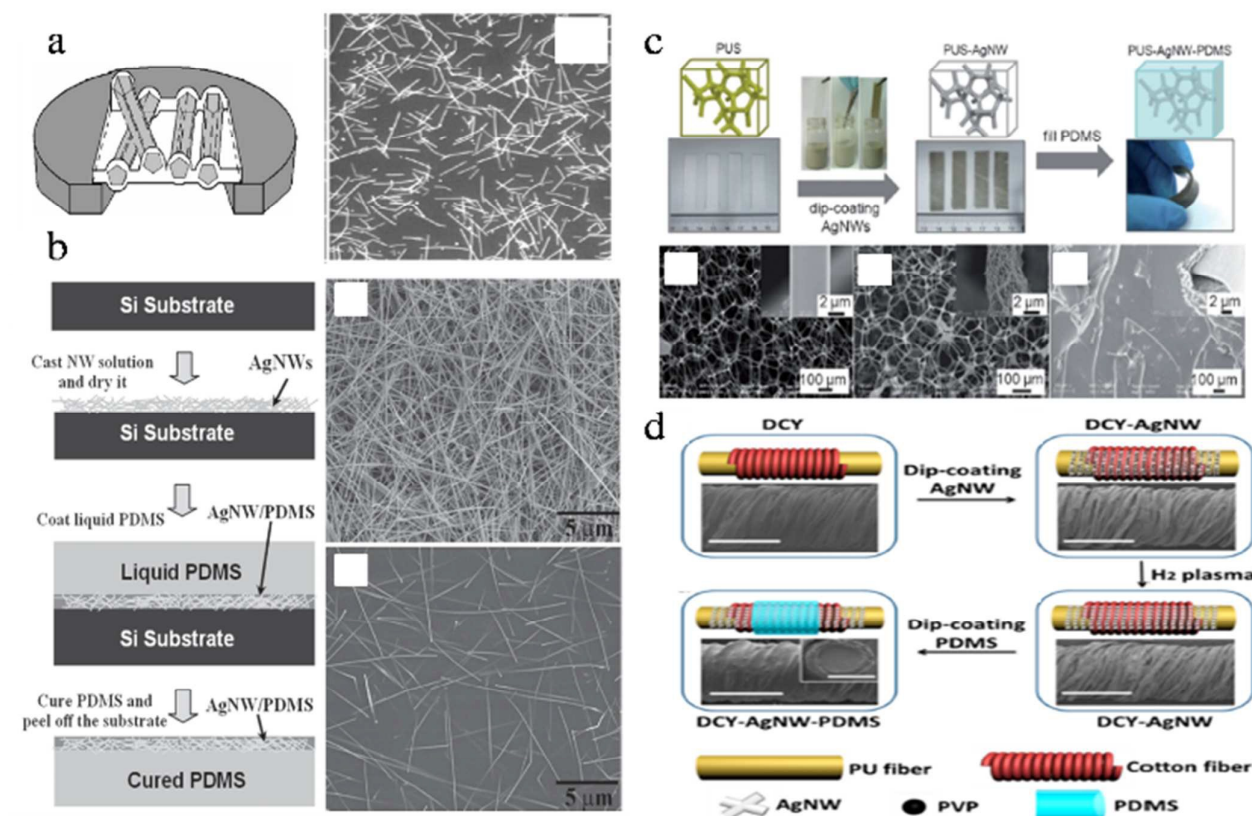


Fig. 3 a) Stretchable conductor using AgNW. Free standing AgNW-polymer composite by LBL method and associated SEM image⁶². b) Fabrication process of AgNW embedded stretchable film. Upper and lower side SEM images show AgNW deposited on Si and PDMS respectively⁶⁰. c) Synthesis of 3D AgNW composite using PU sponge and SEM image⁵⁵. d) Schematic illustration of composite fibre with yarn and AgNW⁶².

The grooves between the wire coils and the diameter of the rod influence the amount of material needed for coating. Drop casting and spin coating use a centrifugal force to make a thin film, and the spray method uses a fluidic force at high pressure. Rotation speed, material-substrate interaction, material viscosity, and material concentration determine film quality in the drop cast and spin coating process. The NW networks produced by drop casting with improper conditions may show spatial inhomogeneity that is known as a coffee ring effect during the solvent evaporation step. The air spraying method of coating is usually more homogeneous because coating efficiency is mostly controlled by the degree of pressure on the nozzle. Accordingly, the spray method has the advantage of scaling up the coating area and the possibility of depositing a material that has low interaction with the substrate. The choice of solvent, concentration, and adductor, which affects the degree of dispersion of the material, are the dominant factors determining the uniformity of the film. The LBL method is the most homogenous coating technique among these methods. LBL allows the generation of novel nanocomposites with high loading and/or controlled composition, and more precise thickness control at a nanoscale (Figure 3a)⁶⁰. Dip coating or spin coating is used to produce the LBL assembly. A continuous coating using desired material-washing-coating using oppositely charged material-washing process is sequentially performed until the desired

thickness is reached. Polyelectrolyte has an opposite charge material to nanomaterial and therefore strongly bonds with nanomaterial during the coating process, leading to its survival during the washing procedure. Common positively charged poly-electrolytes are poly(allylamine), poly(dimethyldiallylammonium), and polyethylenimine and common negatively charged polyelectrolytes are poly(styrene sulfonate), poly(acrylic acid), and poly(vinyl sulfonate)⁶¹. Stretchable electrodes can be made by the same coating as that used for flexible electrodes, but are more commonly prepared by a transfer and/or embedding technique because of their poor adhesion with polymer. In an embedded technique, AgNWs are simply surrounded by a polymer substrate or a polymer coating. When the strain applied, NWs receive intensive stress in common case, but the embedded NWs can disperse the stress because the strain localization on the AgNW film can be suppressed by the polymer substrate^{29,3}. As a result, the embedded NW film shows high stretchability over flexibility. Figure 3b shows a general scheme to synthesize a stretchable electrode with nanomaterials⁶². AgNWs are drop-casted onto a substrate and then liquid PDMS is casted on top of the AgNW film. After the substrate is peeled off, the resulting AgNW embedded polymer film can withstand 50% tensile strain under $\sim 1 \Omega/\text{sq}$ changes. Moreover, some researchers have produced a stretchable AgNW film using an alternative embedded technique with a dipping method

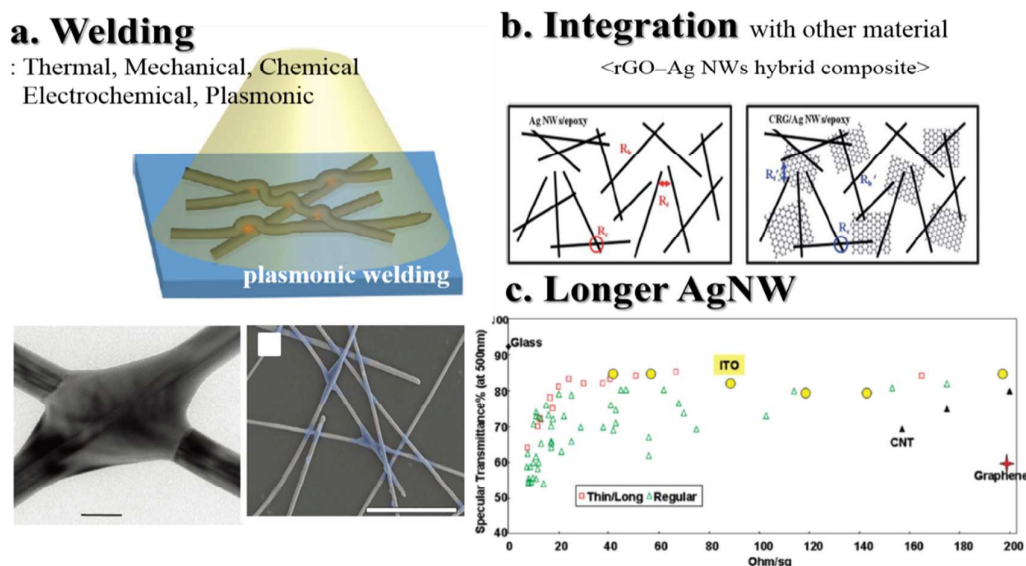


Fig. 4 Three different methods for junction conductivity modulation. a) Representative image of welding process and SEM image of AgNW after plasmonic welding⁷¹. b) Schematic illustration of hybrid composite for enhancing conductivity at junction⁷². c) Transmittance at 500 nm and R_{sh} for long/short Ag NW electrodes⁷³.

instead of drop casting. A 3D foam template with AgNW-PDMS shows 160% resistance change ($\Delta R/R_0$) at 100% strain (Figure 3c)⁵⁵ and a fiber template with AgNW-PDMS exhibits high conductivity (688 S/cm) at 500% tensile strain (Figure 3d)⁶³. In addition to the mechanical strength, the embedded NW film shows a low surface roughness and a high chemical stability. The 1D shape of an AgNW film tends to present a large surface roughness which can trigger an electrical shorting or a high leakage current, but the embedded NW film shows a few nm surface roughness, leading to a highly efficient OLED device¹⁸⁹. In addition, a chemical stability of the embedded AgNW film is demonstrated with an example of an electrochromic device²⁰³. As a result, the embedded AgNW film can be survived in a chemically and mechanically harsh environment during operation

2.1.3. Issues: Junction and Adhesion. NW shows good conductivity along the axis, but exhibits a magnitude greater resistance on the junction side because electrons should be tunnelling quantum mechanically across the stacked NWs. If there are plenty of surfactants on the junction side, it is much harder for electrons to jump into the other NWs. Resistance on the junction, called contact resistance, will be increased depending on the interfacial state between the upper and bottom NWs. According to a computational calculation, a lower contact resistance reduces the sheet resistance⁶⁴. In the real device, the contact resistance is measured over $\sim G\Omega/\text{sq}$. This means that if we can reduce the contact resistance to $100\Omega/\text{sq}$, we can obtain the lowest sheet resistance with same number of NWs. Thus, modulation of the junction side plays an important role not only in terms of the electrical property, but also in terms of surface roughness and optical properties. A rough surface morphology has a crucial impact on the operation of devices; the out-of-plane oriented wires result in poor mechanical adhesion to the substrate⁶⁵, leakage currents⁶⁶, short circuits⁶⁷ and recombination sites in device

systems. Light scattering can be also intensified by a rough surface, leading to increased haze.

There are several methods to solve junction resistance. First, the property of the NW itself can control contact resistance and light scattering (as discussed on page 7). A smaller diameter with a longer length leads to higher conductivity and lower haze (Figure 4c). A Second, a welding technique is the best-known and most widely used method to decrease the contact resistance. The NW junction can be fused by exposing it to extra energy because it will be locally heated up by vibration of the electrons. Direct heating⁶⁸, pressure^{67,69}, potential⁷⁰, and plasmon^{71,72} are candidate energy sources. The remarkable reduction in melting point due to a nanodimension makes it possible to weld NWs at mild temperatures. In their study, Garnett et al. describe plasmonic welding (Figure 4a)⁷¹. Light-induced plasmonics shows an extraordinary behaviour, called a self-limited welding process, compared to other welding process. In the case of plasmonic welding, the heat is generated primarily in the bottom NW and the heat generation efficiency depends on the gap/overlap size. After welding, no more heat generation occurs because the heat from the gap plasmon modes in the wire junction is no longer excited on the welded junction. NWs can join together and further damage can be prevented by the self-limited welding process. Another method is chemical welding, involving post-treatment with chemical compounds or integration of Ag NW with other materials (Figure 4b). This is a much simpler way to modulate a physical property. Gaynor et al. present chemical welding with PEDOT:PSS⁸⁴. PEDOT:PSS enhances contact resistance and substrate adhesion so that a large transparent electrode with good functionality is produced. In addition to conductive polymers, integration of NW with other nanodimensional materials such as TiO_2 ⁸¹ and Au⁴⁷ has been intensively studied. We will introduce and compare integration of NWs with various materials in chapter 3.

Table 2. Surface modification									
Type	Material	Condition	Changes						
Plasma	O ₂ ⁷³		Hydrophilicity (240Ω/ at 86%)						
	H ₂ ⁷⁴	100W, 5S	to heat the samples						
Chemical	Silane	OTMS ⁷⁵	60°C, 24hrs, toluene	Hydrophobicity for film uniformity					
		NH ₂ ⁷⁶	1hrs, baked 120	work function modulation					
		phenyl ⁷⁷	3000rpm, 1hrs, toluene	Improve mobility, hysteresis, and bias stress stability					
	SH	SH ⁷⁸	22°C, 24hrs, ethanol	hydrophobicity,					
		Polyelectrolyte(PDDA) ⁵⁶	PDDA solution	Induce electrostatic interaction					
poly	dopamine ⁷⁹	24 h. and air dried	Hydrophilicity, adhesion						
AgNW Modification									
Type	Material	Condition/Changes			λ	T _{before}	R _{before}	T _{after}	R _{after}
Inorganic	Au ⁴⁷	to reduce R					260Ω(>1G)		220Ω(450)
	AZO ⁸⁰	to reduce R			near	~80	18	~7	12
	TiO ₂ ⁸¹	to prebind AgNWs connection			550	84	>1M	84	19
Ligand exchange	hexylamine ⁸²	homogeneous dispersion with SBS			-	-	σ=1.5kS/c	-	σ=3.5kS/c
	1H,1H,2H,2H-perfluorodecanethiol ⁸³	to disperse in highly fluorinated solvent			550	~82	10	70	48
Stabilizer	perfluorinated methacrylate polymer(EGC-2702) ²³⁴	to disperse in highly fluorinated solvent			550	~82	10	81	10
	Aa-PDA ⁶⁵	to improve adhesion ability of AgNWs			550			89	16.3

The major problem associated with making a NW film is a weak adhesion of the NWs to the substrate. The random arrangement of the NW network results in peak-to-peak roughness that is 2-fold higher than the diameter of NW. Adhesion of the NW layer to the substrate plays a critical role in the surface roughness and homogeneity during the coating process and this determines a mechanical properties as well as electrical and optical properties of NW. Mechanically, low adhesion of the network to the substrate causes large friction on the NW, leading to failure at low strain. Electrically and optically jointed junctions formed by strong adhesion between NW and the substrate show high conductivity and low haze. Such strong adhesion can be developed by surface modification of the substrate or the material itself. Plasma treatment^{73,74,75} and chemical treatment^{76,77} are well-known techniques to modify the substrate surface. Our group demonstrated a highly conductive AgNW film with high transmittance using plasma treatment(Figure 5a)⁸⁵. Plasma treatment alters a hydrophobic PET substrate to a hydrophilic one. An ultrathin 2D GO layer can tightly hold AgNWs though a strong interaction between the hydrophilic GO layer and hydrophilic PET. A chemically self-assembled molecule on the hydrophilically modified substrate causes a similar effect. Furthermore, our research group was able to fabricate a stretchable transparent electrode⁸⁶. Silane molecules with a terminal amine functional group are coated on PET using a self-assembly technique. Amine functionality induces strong complex-type bonding with AgNW so that the strongly adhered AgNWs prevent hydrophobic recovery of PDMS, resulting in a uniform and stable film conformation. In another paper, PDDA, which is a cationic polyelectrolyte, is used to enhance an adhesion by electrostatic interaction⁵⁶. Likewise,

numerous studies on surface modification methods for the substrate and nanomaterial have been published. The surface modification methods for substrate and NW are introduced in Table 2.

Modified NW has been investigated to produce a highly stretchable electrode. Functionalization of NW is not easy, but can be partially modulated by stabilizer, a self-assembly technique using silane or thiol molecules, and ligand exchange to alter the outer capping agent to another functionality. Figure 5b shows a tailed NW with hexylamine formed by a ligand exchange process⁸². The NW with hexylamine is necessary for a homogenous dispersion of AgNWs in styrene-butadiene-styrene (SBS) elastomer because SBS elastomer is only dispersible in nonpolar solvents. As a result, the mesh heater with modified AgNW shows stable resistance changes and joule-heating characteristics under 30% strain over 5,000 cycles.

Here, we compare the electrical, optical, mechanical properties before and after improving the junction resistance. It is suggested that the resistance of NW proportionally decreased as the NW junction is reduced, but transmittance doesn't show a pronounced effect. It is because the junction area only covers approximately 1% (average nanowire spacing of approximately 1 μm). However, a scattering light is influenced by junction state. The scattering efficiency in dark field microscopy (related to back scattering) demonstrates the linear relationship with the reduced junction resistance. In case of a haze factor (related to forward scattering), a haze value decreases even with small numbers of AgNW junctions. AgNWs with a small diameter show almost similar transmittance with AgNWs with a large diameter when the resistance is same, but the haze factor with the small diameter

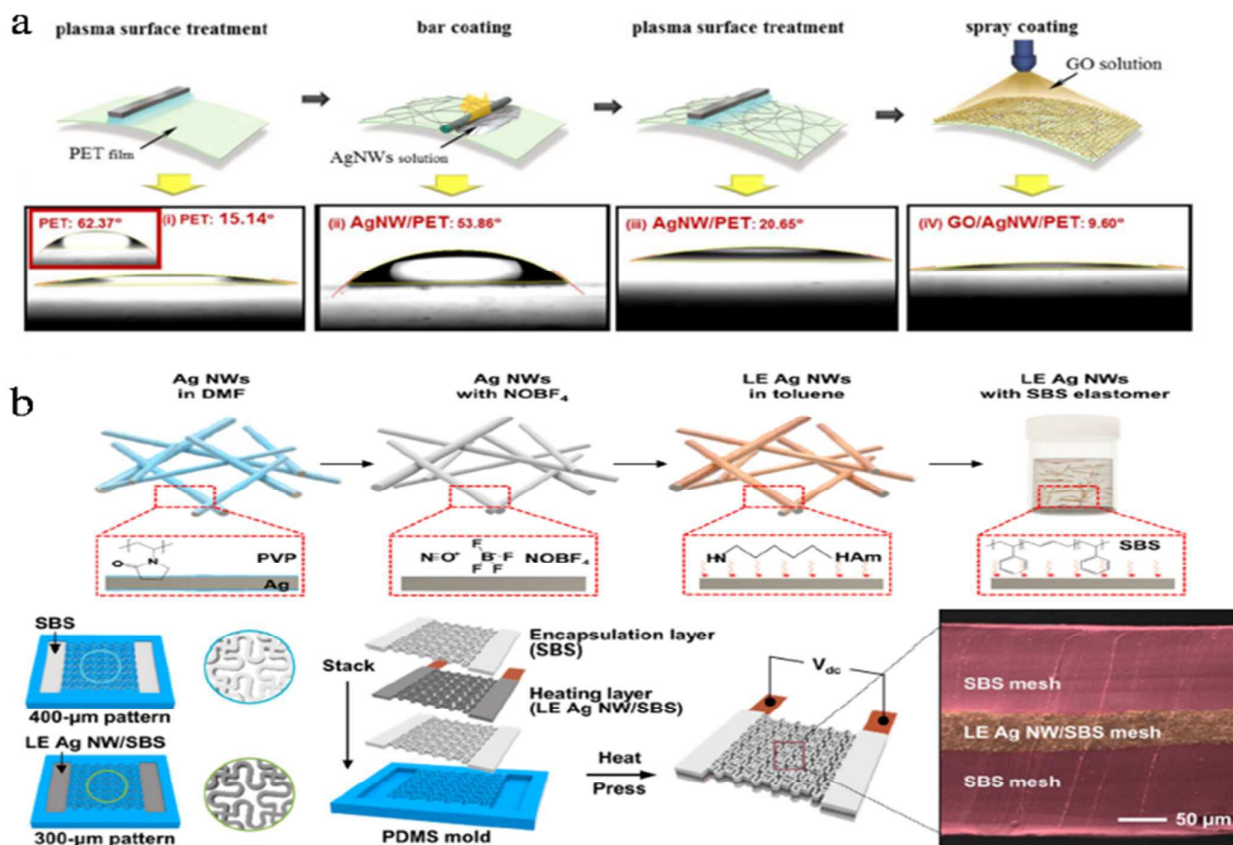


Fig. 5 a) Schematic fabrication process for AgNW transparent electrode with GO overcoating layer and associated water contact angle to confirm hydrophilicity of surface⁸⁵. b) Fabrication step of ligand-exchanged AgNW and the mesh heater with their AgNWs. The stretchable heater is composed of encapsulation layers (SBS) and a heating layer (Ag NW/SBS).

depicts twice smaller than that of the long diameter. Thus, AgNW junction state can modulate the haze degree of the AgNW film. Our group demonstrated that AgNWs with a GO coating layer showed lower haze than that without the GO coating layer⁸⁵. The GO coating layer reduces the AgNW junction resistance. The mechanical strength of the AgNW film is also affected by the AgNW junction state. When AgNW networks are wrapped with the GO layer that leads to improving a junction adhesion, the resistance of the AgNW film decreases from $R/R_0=7$ to $R/R_0=2$ and the stretchability increases.

2.1.4. Research trend of NW. AgNW can be synthesized by two different ways: a template assisted method and a solution-phase method. In case of the template assisted method, anodic aluminium oxide²⁹⁷, porous materials²⁹⁸, carbon nanotubes²⁹⁹, block copolymers³⁰⁰, DNA chain³⁰¹, rod-shaped micelles²⁹⁸, and calix[4]hydroquinone nanotubes³⁰² have been used as a template. Most cases among the template assisted method produce AgNW with high aspect ratio and homogeneity, but some problems such as a complex procedure and a small amount are still remained. In contrast, the solution phase method synthesizes AgNW with reduction of AgNO₃, which is appropriate to a large scale production. The important thing in this method is the role of the capping

molecules. They prefer to attach specific facet so that an isotropic growth of Ag is encouraged. In a previous time, this method shows limitations in making a high aspect ratio of AgNW, an irregular shape or length, and a polycrystalline domain structure. However, endless efforts for developing a capping agent and a reductant agent enable to produce high quality of AgNW even with a solution phase method. Furthermore, to reduce the cost issue of the metal NWs, the copper nanowire (CuNW) regards as a substituent of AgNW due to its extremely low cost with a comparable conductivity. For that reason, there have already been plenty of studies how to make a commercially available CuNW. Aaron R. Rathmell et al. produces a long and well dispersed CuNW solution using PVP instead of ethylenediamine (poor dispersant for the CuNW)²⁹⁵. Others also suggest new synthetic procedure for ultra-long single crystal using hexadecylamine and cetyltrimonium bromide²⁹⁶. In current, the length and dispersibility issues are intensively investigated and some parts are solved. However, several disadvantageous properties including a reddish color that leads to a low transparency (1), a poor crystallinity (2), a low yield (3), a non-linear morphology (4) and a rapid oxidation under ambient condition (5) must be still enhanced for the real applications. One possible candidate for the quick application, called cupronickel NW, has been introduced. The cupronickel NW consists of a core CuNW

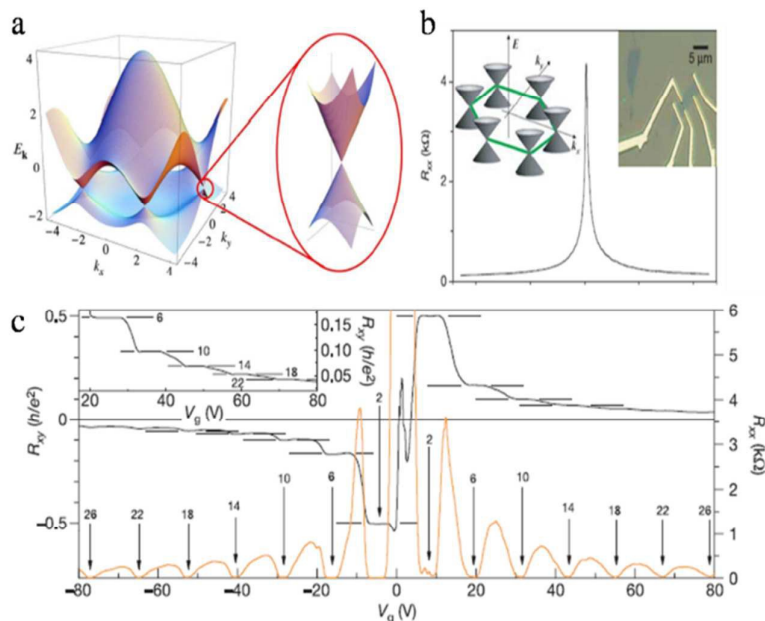


Fig. 6 Electrical properties of graphene. a) Electronic dispersion diagram of graphene²³³. b) Resistance changes depending on gate voltage. c) Hall resistance_{xy} (black) and magnetoresistance (red) versus gate voltage. Half-integer quantum Hall effect is presented²³⁴.

with a Ni shell. The conductivity of this material is dominantly originated from CuNW, leading to high conductivity while Ni effectively protects Cu from any oxidation environment, resulting high oxidation stability. In addition, Cu:Ni(2:1) depicts neutral gray color, making them more suitable for practical application²⁹⁴.

Another research trend of AgNW is to produce commercial products. AgNW exhibits extraordinary conductivity compared to other new materials, so many practical applications have been suggested. Especially, AgNW is favored in large area device because of an easy coating processing with a high conductivity. In large area device, the high conductivity should be maintained on whole area. The most widely used solution is embedding technique, which is already introduced in page 4. For example, the prototype of an organic light emitting diode (OLED) and a touch screen for large area display, smart window, and large area solar cell have been attempted. The flexible optoelectronics such as OLED, solar cell, touch screen, electrochromic, and sensor have been presented (in details in chapter 4). Until now, however, most examples using AgNW show a relatively poor device performance in comparison with the conventional commercial product. The detrimental factor of this poor device performance is considered as a surface roughness of the AgNW film and its easy oxidation on harsh environment.

2.2. Two-dimensional graphene

2.2.1. Dirac fermion. 2D nanomaterials exhibit electron transport as described by a Dirac-like equation rather than a Schrodinger equation because of their quasi particle behaviour. The electrons on 2D materials follow relativistic quantum phenomena and the electron wave propagates through the layer of 2D material. Graphene is composed of a single layer of atoms and also follows Dirac physics, with p orbital Dirac fermions (Figure 6a,b)^{87,88}. The most interesting phenomenon

of graphene is its electronic spectrum. The valence band and conduction band of graphene join at a single point at the Fermi level in momentum space, which is called the Dirac cone. The Dirac cone provides great charge carrier mobility and zero effective mass near the point of charge neutrality. At room temperature, electrons propagate through the honeycomb lattice and travel for micrometres without scattering⁸⁹. Graphene placed on an atomically rough substrate shows electron propagation without scattering at room temperature, resulting in sensitivity to neighbouring materials such as dielectrics, superconductors, ferromagnetic, and dopant. As a result, electrons of graphene exhibit unusual behaviour such as tunnelling⁹⁰, confinement^{91,92}, quantum effects at room temperature⁹³, and integer quantum Hall effect⁹³ by spin-orbit coupling. Electronic property can be modulated by an external electric/magnetic field and graphene geometry. Young Tak Lee et al. demonstrated that graphene is a good candidate as a source/drain electrode for

vertical FET since it has excellent electrostatic integrity due to the 2D nature of the system⁹⁴. However, the most interesting physical property of graphene is

its huge carrier mobility ($\sim 200,000 \text{ cm}^2 \text{V}^{-1} \text{s}^{-1}$) with zero band gap⁹⁵. To improve the conductivity of graphene films, the carrier concentration should move away from the Dirac point, where the density of states is zero. Physical and chemical doping is often used to modulate graphene mobility. H^+ and OH^- on the graphene backbone can result in poorly conductive graphene because of localized states close to the charge neutrality point. Moreover, weakly attached dopants are able to act as donors or acceptors⁹⁶. This changes the carrier concentration of graphene and leads to high conductivity. In addition to material changes, strain and deformation also affect the electronic, optical, and phonon properties of graphene. Seon-Myeong Choi et al. reported that the metallic nature is maintained to a uniaxial strain of 30% and the work function also increases with both the uniaxial and isotropic strain increase⁹⁷.

In addition, graphene has been spotlighted as a soft electrode due to its outstanding optical properties. The thickness of graphene is far less than the wavelength of light so light absorbance by the material becomes very small. Graphene absorbs in significant light ($\pi\alpha=2.3\%$) and results in 97.5% transmittance and negligible reflectance (<0.1%) for monolayer graphene⁹⁸. Four-layer graphene shows 89.4% transmittance because light absorption is linearly proportional to the number of layers⁹⁹. Another interesting optical property is high transmittance in the visible region but low transmittance near the ultraviolet region for multilayer graphene, which is attributable to inter band electronic

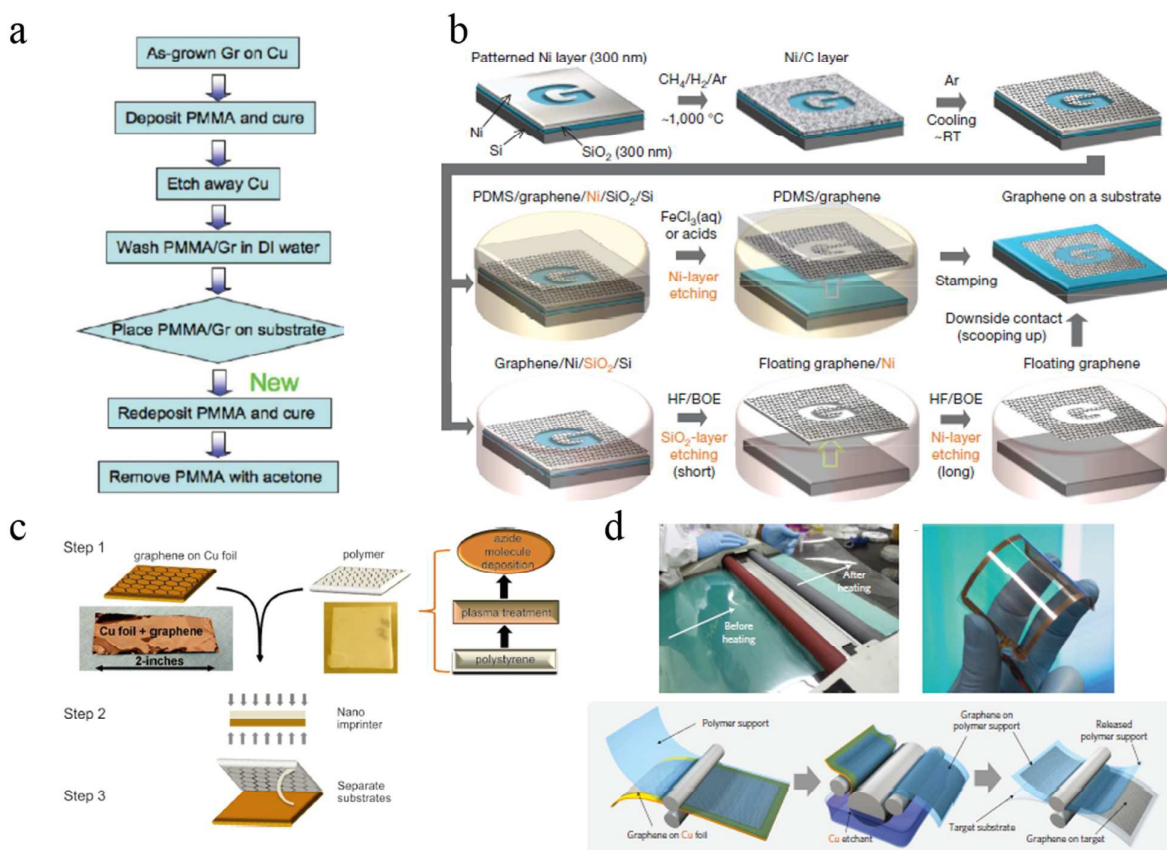


Fig. 7 Schematic depiction of various transfer methods. a) PMMA assist transfer printing method¹⁰⁰. b) PDMS assist dry transfer²¹. c) azo molecule assist dry transfer¹⁰⁶. d) Roll to roll

transition from the unoccupied π^* states (~ 250 nm)¹⁰⁰. However, graphene still exhibits good physical properties as transparent electrodes because of uniform transmittance with a large wavelength window compared with an ITO film¹⁰¹.

2.2.2. Coating Method. Among graphene derivatives, CVD graphene is widely used as a soft electrode material because of the inexpensive and readily accessible approaches for obtaining a high-quality graphene. A CVD graphene metal catalyst must be transferred onto a desired substrate to act as an electrode. The transfer method is one of the important parameters determining the quality of graphene because a high-quality graphene from the synthesis step can be degraded during the transfer process. Transfer is typically performed in two different ways: wet transfer or dry transfer. In the case of wet transfer, graphene is first coated with polymer supporter and the metal catalyst is removed by etchant (FeCl_3 in HCl , $\text{Fe}(\text{NO}_3)_3$ in H_2O , $(\text{NH}_4)_2\text{SO}_8$ in H_2O). Graphene is transferred onto the desired substrate after washing with H_2O several times and then the polymer supporter is also etched. During the wet transfer process, the etching rate, the type of supporter, washing process with H_2O , and polymer etchant conditions are important. Rapid etching and consequential generation of bubbles lead to cracks or wrinkles on graphene. Few micrometre cracks have been observed when graphene on Ni is etched by nitric acid, which is a stronger etchant than $(\text{NH}_4)_2\text{SO}_8$ or FeCl_3 ¹⁰². Even though every polymer supporter is

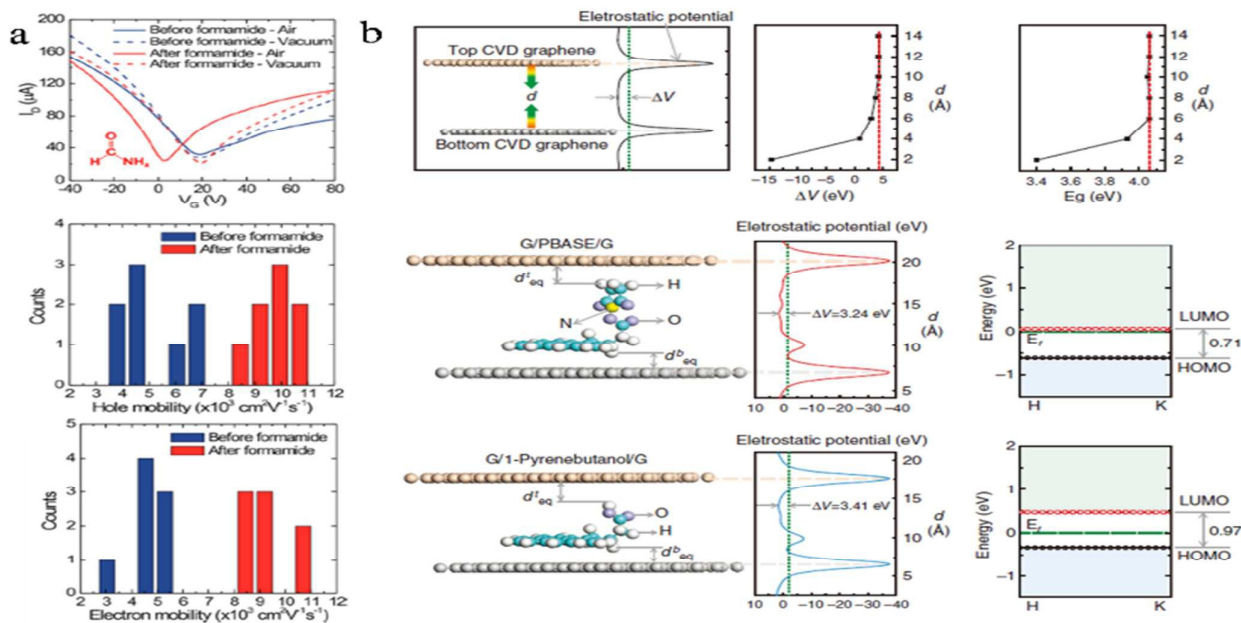
used to facilitate free standing of graphene during transfer, each polymer undergoes different mechanism to transfer graphene. PDMS, which is a well-known molecular stamp, maintains low adhesion with graphene so the target molecule can be transferred from PDMS to the desired substrate (Figure 7b)²¹. PDMS transfer requires a long etching time, but induces minimum polymer residuals. PMMA is another widely used polymer supporter. PMMA forms strong bonding with graphene, thus preventing graphene damage during the metal catalyst etching process. Hence, the Rouff group found that PMMA can cause cracking or wrinkling during the PMMA removal process (Figure 7a)¹⁰³. The PMMA coating holds graphene rigid as it forms covalent bonds with it. The ripple on graphene that is generated during the growth and cooling process is maintained and hinders contact between graphene and substrate, leading to tear off in polymer removal procedure. To overcome this problem, they propose an additional PMMA coating before PMMA removal; a second PMMA layer redissolves the original PMMA and relaxes the wrinkles in graphene. As a result, the additional PMMA coating successfully yields high-quality graphene. The important component of the wet transfer method is the polymer or etchant residue, which affects the physical properties of graphene. Suk et al. studied the effect of polymer residue (Figure 8a)¹⁰⁴ and found that PMMA at high concentration can maintain high P-type doping I-V

characteristics after polymer washing, and that amide treatment easily recover the original I-V characteristic through electron donation of formamide in the polymer residue. A heating method of graphene to remove polymer residue under an Ar/H₂ environment was also introduced. Recently, to enhance the poor electronic coupling by polymer residues Christian and co-workers incorporated 1-pyrene butyric acid between the top and bottom graphene layers (Figure 8b)¹⁰⁵. Plane-to-plane tunnelling conductivity of stacked CVD graphene layers was improved by 6 orders of magnitude after pyrene derivative insertion compared with the original graphene. To minimize damage to graphene, many dry transfer methods have also been attempted. Lock et al. used linker molecules to detach graphene from metal catalyst (Figure 7c)¹⁰⁶. Azide molecules as a linker are spin-coated on the oxygen plasma-treated polymer substrate and then graphene is attached onto the modified substrate. After applying heating and pressure, azide molecules form carbene with the graphene backbone. Strong bonding between graphene and substrate allows clean detachment of graphene from the metal catalyst during transfer. Yoon et al. introduced the use of epoxy to peel off graphene in a similar way¹⁰⁷. Another strategy called the “roll to roll process” was demonstrated by Sukang Bae et al. to fabricate a large-area graphene electrode (Figure 7d)¹⁰⁸. The graphene film on Cu foil and a thermal release tape are inserted together between rollers with soft pressure. After the Cu foil is etched, graphene is attached to a polymer substrate with thermal release tape by mild heating between rollers, yielding 30-inch graphene with 125 Ω/sq is developed. However, this method can cause damage to the graphene by shear stress caused by the rolling speed or rigidity of the substrate and low conductivity due to

the polymer residue. As a result, the hot pressing method is suggested as a new transfer method¹⁰⁹.

On the other hand, through chemical exfoliation many graphene derivatives such as graphene flake solution^{110,111}, graphene oxide (GO), and reduced graphene oxide (rGO) can be produced. These graphene derivatives show much lower electrical properties than the CVD grown graphene, but their low cost, easy handling, possible functionality, and various applications make them interesting. Chemically exfoliated graphene can easily generate an ordered film by LB¹¹², drop casting¹¹³, spin coating¹¹⁴, dip coating¹¹⁵, spraying¹¹⁶, Meyer rod coating¹¹⁷, LBL¹¹⁸, vacuum filtration deposition¹⁰⁰, and electrohydrodynamic jet printing¹¹⁹. Laura J Cote fabricated a monolayer of GO by LB assembly without a surfactant or stabilizing agent¹¹². Strong electrostatic repulsion between edge-to-edge and face-to-face graphene prevents overlapping and stacking of graphene sheets during LB assembly. A GO film made by the above method guarantees high uniformity because of the formation of stable colloidal suspensions in water through oxygen functional groups¹²⁰. In addition, a porous electrode can be simply fabricated by modulation of GO-solvent interactions. Our research group proposes a GO film with non-stacked porous structure produced by vacuum filtration using an anti-solvent method. A porous rGO electrode gives a high surface area (1435.4 m²/g) and high conductivity, which is appropriate for use as an electrode in a supercapacitor (Figure 9a)¹²¹. However, it is hard to make a good film directly using rGOs or graphene flakes due to strong van der Waals interaction between graphene sheets, and in general preparation of GO film by chemical/thermal reduction is preferred. Figure 12a,b depicts the electrical property of rGO film depending on the coating method. Subsequently, our

Fig. 8 a) I_D-V_G characteristics for graphene field effect transistor indicating Dirac point changes before (Blue) and after formamide treatment (Red)¹⁰⁴. b) Electronic properties of graphene/molecule/graphene electrode and DFT-stimulated structure. Typical electrostatic potential and tunnelling barrier height (ΔV) are calculated for various molecules sandwiched by graphene¹⁰⁵.



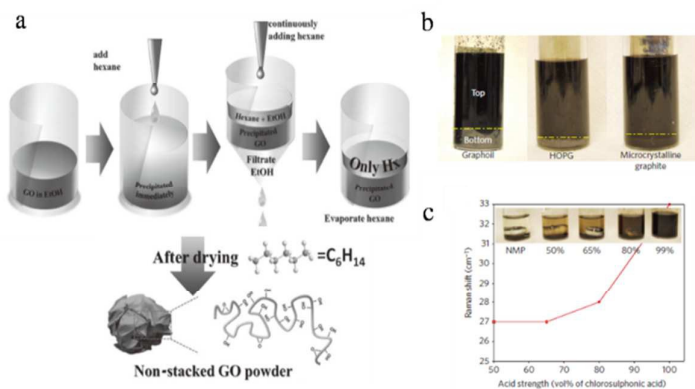


Fig. 9 a) Schematic illustration of the fabrication of porous non-stacked GO¹²¹. b) Photograph showing solubility of superacid-driven exfoliated graphene. Graphite, HOPG, or microcrystalline graphite is used as an initial graphene source. c) Raman shift at G band as a function of acid strength. Raman shift is examined to predict the degree of protonation of graphene¹²⁴

group developed a direct rGO coating method to avoid the need for a post treatment that can damage an active material. The GO suspension is reduced by 5.0 μl hydrazine solution with 35.0 μl ammonia and the solution is placed in a water bath at 95 $^{\circ}\text{C}$ for 1h. Ammonia solution prevents aggregation of rGO during reduction, leading to formation of a uniform and thin rGO film. Finally, the rGO electrode is deposited on the substrate by spin coating or spray coating to give a highly conductive thin electrode for use in molecular electronics^{122,123}. Moreover, the Pasquali group demonstrated a direct coating technique to produce densely packed graphene fibres and sheets using the proper solvent (Figure 9b)¹²⁴. A strong acid (chlorosulphonic acid) protonates graphene so that graphene flakes in superacid undergo competition between short-range repulsion and long range attraction, resulting in a well-dispersed and highly concentrated graphene or rGO solution. As a result, transparent conducting films (1000 Ω/sq with 80% transmittance) are produced with uniform and large liquid crystal domains. A functionalized rGO film for a flexible electrode has also been proposed. The advantage of functionalized rGO is the ability to make homogeneous colloidal suspensions using special functional groups to provide functionality to enhance adhesion on the substrate and to improve conductivity by a doping effect. Choi et al.¹²⁵ produced a functionalized rGO film through self-assembly of the hydrophobic backbone of nafion that shows high conductivity of around 1176 S/m, good electron transfer characteristics, and low interfacial resistance in the bio-sensor.

2.2.3. Issues: CVD graphene. High sheet resistance is one of the most important factors influencing the poor performance of electronic devices that use transparent electrodes based on graphene. In theory graphene has remarkably high conductivity, but the real conductivity is 3 orders of magnitude lower than the expected value because of grain boundaries, defects, and oxygen-containing groups in the graphene sheet. Strategy to improve the conductivity of the graphene films are to control the degree of grain boundaries, control the topography of graphene such as wrinkles, edges, and defects, and to incorporate a conductive material into them (doping or hybrid composite). First, high-quality graphene with a large

grain domain have been researched by high-throughput approaches for graphene synthesis. A single crystal metal catalyst normally ensures high-quality of graphene. Gao et al. synthesized millimetre-sized single-crystal graphene on a Pt single crystal metal catalyst by ambient pressure CVD. The graphene showed a low wrinkle height and huge carrier mobility (7100 cm^2/Vs) under ambient conditions¹²⁶. Furthermore, the type and flow rate of carbon source¹²⁷, growing temperature¹²⁸, and partial pressure of hydrogen¹²⁹ also affect the size and morphology of the graphene domain. Second, various coating techniques (transfer and deposition) have been tested to modulate the topography and morphology of graphene such as wrinkles, cracks, and edges. Wrinkles, cracks, and edges of

graphene are known as scattering sites and prevent charge transport by limiting the electron mean free path, leading to low conductivity. In the case of CVD, transfer-induced defects are dominant in affecting electrical properties. As mentioned earlier, reactions during the etching of Cu can cause cracking in the graphene film and degrade the carbon sp^2 network. Thus, the choice of a proper etching solution and transfer method is significant. Finally, doping is often used to enhance the conductivity as a result of an increase in carrier densities. Doping of graphene may be simply classified as electrical doping (achieved by changing gate voltage) and chemical doping (obtained using chemical species). Chemical doping can be further divided into physical adsorption and chemical adsorption. Physical adsorption with gas, metal, or organic molecules does not disrupt the structure of graphene. The relative position of density of states of the highest occupied molecular orbital (HOMO) and lowest unoccupied molecular orbital (LUMO) of the dopant and the Fermi level of graphene affect the electronic property of modified graphene¹³⁰. When the HOMO of a dopant is above the Fermi level of graphene, the dopant acts as a donor, with carrier transfer from the dopant to the graphene layer. Electron withdrawing groups adsorbed on the surface generally exhibit a p-type doping effect, whereas electron donating groups show an n-type doping effect. Characteristics of doped graphene depending on dopant are demonstrated in Table 3. Surface transfer doping by acid treatment such as H_2SO_4 , HCl, HNO_3 is well-known for a p-type dopant and can enhance the charge transfer and conductivity of graphene. A 4 layer graphene film with HNO_3 treatment shows 30 Ω/sq with 90% transmittance, which is comparable to ITO¹⁰⁸. Chemical adsorption involves the substitution of carbon atoms in graphene by atoms with a different number of valence electrons, such as nitrogen and boron. Chemical adsorption is achieved by direct synthesis (CVD, segregation growth, solvothermal method) and post-synthesis treatment (thermal, plasma treatment)¹³¹. Interestingly, substituted nitrogen affects the charge distribution of carbon atoms so that the Fermi level moves above the Dirac point, resulting in band gap opening. Thus, N-

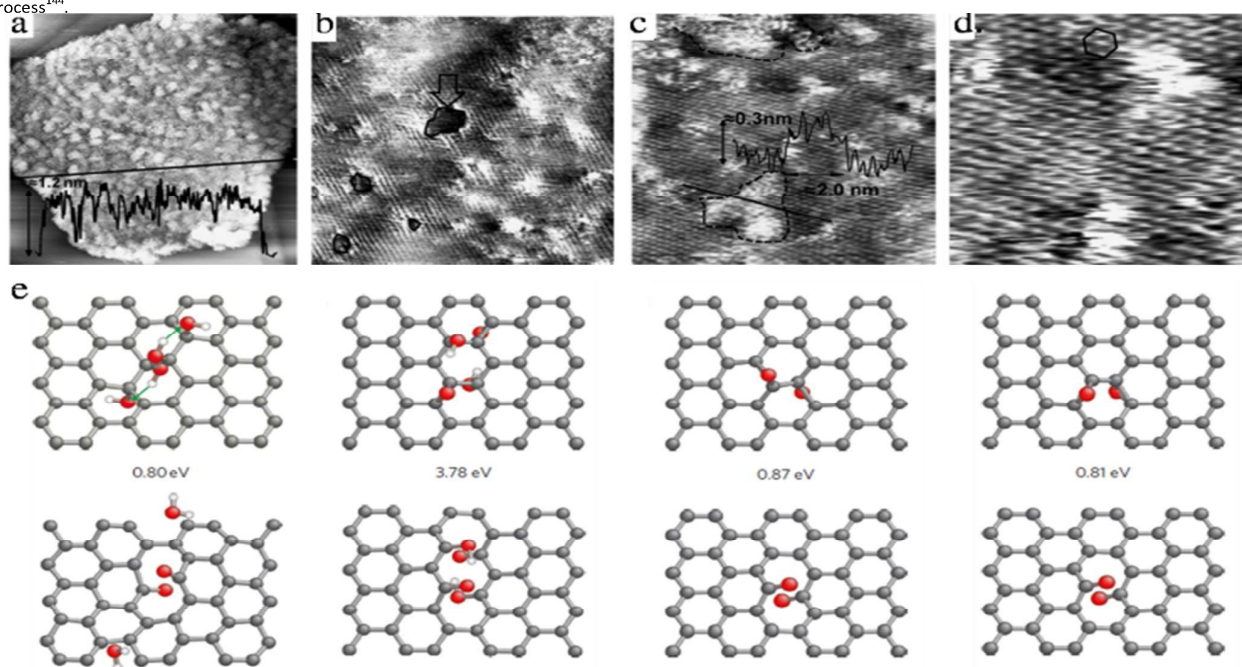
doped graphene is better for application in semiconductor devices than in electrodes.

2.2.4. Issues: rGO. The rGO electrodes provide several advantages: 1) One-phase reaction is possible without additional surfactant because of water-soluble properties, 2) The homogeneity and composition of the films are simply determined by the composition of the parent suspension and surface modification of the substrate, 3) rGO film with various morphology and functionality such as dispersability, adhesion, work function, and conductivity can be fabricated by low temperature and high throughput processing, 5) Work function of rGO (4.2–4.6 eV) correlates with the HOMO level of most of the organic materials that are used in layered structure devices such as solar cells, light emitting diodes (LEDs), and sensors. However, the biggest problem associated with rGO electrodes is the relatively low conductivity compared with CVD graphene due to the large number of defects on the sp² domain. Such effects are generated during the oxidation and reduction process. The average domain size of graphene (L_D) is estimated by the Raman intensity of D (I_D) and G bands (I_G) of the rGO film using the equation: $L_D^2 = (1.8 \pm 0.5) \times 10^{-9} \lambda_L^4 \left(\frac{I_D}{I_G}\right)^{-1}$ ¹³², Where λ_L is the excitation laser wavelength. The average domain size of graphene is only 2.5–6 nm and sp² domain coverage is less than 60%. Because there are many defects in rGO sheets, space charge limited conduction and coulomb blockade effects are observed in real devices. The physics of rGO electrodes are more similar to those of a graphene quantum dot array than to graphene itself. sp² domains behave like quantum dots whereas oxidized domains act like tunnel barriers such that electrons are transported by a hopping mechanism among

localized states¹³³.

To enhance the conductivity of rGO and recover graphene like behaviour (long-range ballistic transport), repair of any defects is necessary. Defects can be recovered with certain post-treatments such as heating¹³⁴ or functionalization. Oxygen-containing groups on GO become a defect site during reduction. Chemical, electrochemical, photocatalytic reduction, flash conversion, and heat treatment above 200 °C have been tested for recovery. For chemical reduction, various reducing agents are used including hydrazine¹³⁵, hydrides¹³⁶, dimethyl-hydrazine¹³⁵, hydrides¹³⁶, dimethylhydrazine¹³⁷, NaBH₄¹³⁸, AlCl₃¹³⁹, iodic acid¹²², hydroquinone¹⁴⁰, and *p*-phenylene-diamine¹⁴¹. Each reagent shows different degree of reduction, resulting in different C/O ratios and conductivity. Hydrazine is effective for removal of in-plane functional groups (epoxy, hydroxyl) but not for the edge moieties (carboxyl and carbonyl). However, many oxygen groups still remain after chemical reduction. Thermal treatment is known to be a high recovery method. The C/O ratio obtained by XPS spectra of chemical and thermal reduction is 8.8 and 14.1, respectively¹⁴². However, during the heating, melting can occur at sites of defective pairs and small lateral size, preventing sp² recovery. Thus, the combination of chemical and thermal reduction is more efficient than reduction by any one process. Our group investigated structural information on the single rGO and the influence of atomic dopants during thermal treatment¹⁴³. Chemically reduced rGO showed quite high topographical fluctuation and rGO treated with only thermal reduction exhibited many defect sites due to the removal of oxygen groups (CO/CO₂) in Figure 10a–d. However, post-thermal treated chemically reduced rGO resulted in the

Fig. 10. a–d) Scanning tunnelling microscopy images of chemically reduced rGO by hydrazine(a), thermally reduced rGO(b), reduced rGO with both techniques(c), and high-magnification observation of reduced rGO with both techniques(d)¹⁴³. e) DFT calculation of formation energies and structures of defect after reduction process¹⁴⁴.



formation of crystallized patches because cyclic ether (-O-) groups on graphene can be formed at the edges of wrinkles in a buckle-type fold upon thermal treatment. Chowalla et al. also predicted that the healing mechanism of hydrogen atoms is through reduction of hydroxyl and epoxy groups to highly stable carbonyls and ether groups (Figure 10e). Desorption of hydroxyl and epoxy groups generates CO₂ and CO gases at low temperatures, leading to defective graphene formation, whereas thermal treatment with hydrogen transforms initial hydroxyl and epoxy group to carbonyl and ether groups, which prevents defective reduction of GO¹⁴⁴.

Reduction of functionalized GO is possible to fabricate a rGO electrode with the desired band gap and/or conductivity by

rGO-Ag with PVDF shows a significant increase in AC conductivity when the rGO-Ag content is 2wt%.

2.2.5. Issues: Graphene chemistry. Graphene chemistry is another interesting issue in the graphene field that has not yet been fully explored, although several outstanding features of the chemistry of graphene have been introduced: 1) surface chemistry sensitive physical property, 2) local reactivity changes depending on strain and curvature, 3) periodical absorption of molecules. We can obtain desired properties of graphene using the appropriate specific chemistry. In some cases, even though conductivity losses occur, functionalization of graphene may be used to improve solubility, processability, and other specific properties to facilitate the practical

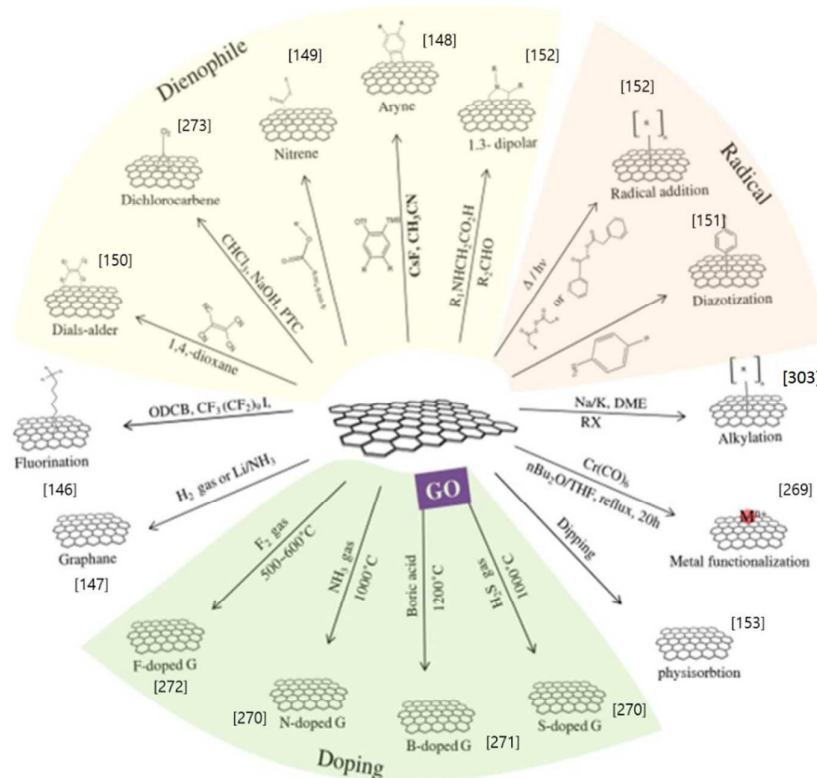


Fig. 11 Types of chemical reaction with graphene derivatives.

the formation of a donor-acceptor complex with graphene. Tuning its work function to match the interface and/or active materials is important to decrease contact resistance in the device and/or enhance the collection and transfer of electrons to the collecting electrode. Functionalization of GO is much more convenient than that of graphene because of the highly active oxygen functional group. Functionalization with nanoparticles, organic materials, and polymers has been proposed for GO-based electrodes. Fu-An He et al. suggested Ag nanoparticle (10–100 nm)-decorated rGO prepared using an in situ method¹⁴⁵. (3-mercaptopropyl) triethoxysilane functionalized GO in DMF is mixed with HAgCl₄, sodium citrate, and ammonia solution, and then hydrazine is added to reduce GO and Au ions simultaneously. The consequently obtained

utilization.

Chemical functionalization of graphene can be achieved using graphene flake, rGO, CVD graphene, and GO. With the exception of GO, all of these undergo similar reactions such as alkylation, fluorination, hydrogenation, doping, and physisorption because they react with the π electron on the graphene basal plane and edge plane. These reactions are shown in Figure 11. Graphene flake shows better solubility, but smaller size and less mobility due to larger defects, and higher inhomogeneity than CVD grown graphene. Interestingly, graphene flake, unlike CVD graphene, can be diversely functionalized because of the larger number of more active edges and defect sites. The merit of graphene flake is its ability to be modified by solution processes and numerous transfer procedures such as spin coating, spraying, and nanoprining.

However, graphene flake can be re-aggregated due to strong preferential bonding site to the graphene plane (i.e., directly

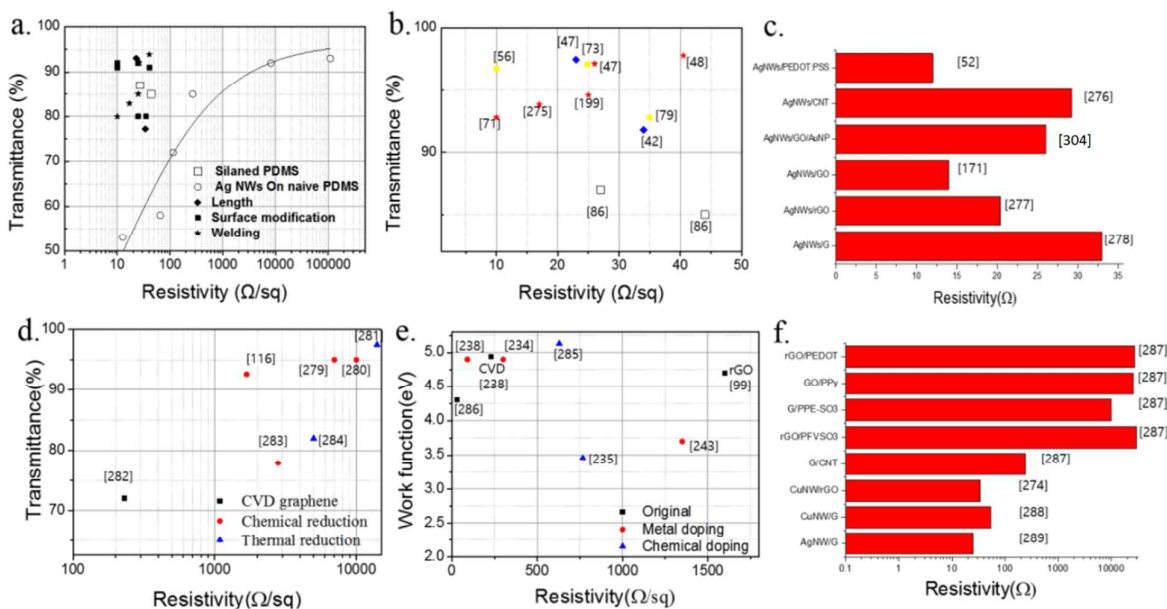


Fig. 12 Comparison of electrical properties of (a,b) representative AgNW electrode. b) Enlarged graph of (a). c) Resistivity of various hybrid composites using AgNW. d) Comparison of electrical properties of representative graphene electrodes. e) Work function and resistivity according to the type of doping on graphene. f) Resistivity for various hybrid composites using graphene.

van der Waals interaction and a dispersant or surfactant is normally used to prevent aggregation of graphene, although this can affect the yield of the reaction. In contrast, CVD graphene is modified by surface reaction after transfer onto the desired substrate. Only the upper surface of graphene reacts with reagent, and the reaction mainly changes the basal plane of graphene by fluorination¹⁴⁶, hydrogenation¹⁴⁷, cycloaddition by arylene¹⁴⁸, nitrene¹⁴⁹, Diels-Alder reaction¹⁵⁰, and alkylation by diazotization¹⁵¹, radical reaction¹⁵² as well as physisorption¹⁵³. Alkylation and fluorination of both CVD graphene and graphene flake damage the π electron state and lead to decreased conductivity whereas physisorption maintains the electrical property of graphene. Thus, physisorption is widely used to develop graphene-based electrodes. π - π stacking or van der Waals interactions influence the physisorption of graphene. Mostly, molecular assembly occurs during physisorption on graphene. Molecules with strong directional bonds such as coordination bonds or hydrogen bonds produce porous assemblies on graphene, whereas weak bonds such as halogen-halogen and van der Waals interactions produce a densely packed array^{154,155}. Adsorption of pyrene and derivatives, tetracyanoquinodimethane (TCNQ), sulfonated poly(aniline) (SPANI), perylene derivatives, poly(styrene sulfonate) (PSS) and other aromatic species has been successfully studied. Moreover, physisorption of certain molecules such as PBASE suggests that the hydrophilic character, work function, and device performance such as power conversion can be improved¹⁵⁶. Furthermore, one proposes non-covalent functionalization of graphene using self-assembly of alkane amines¹⁵⁷. Amine anchor group-graphene interactions and inter-chain interactions between molecules stabilize self-assembly on graphene. Amine has no

over an atom versus the centre of phenyl rings) and a small net charge transfer to graphene, leading to stable formation of an aminodecane layer at room temperature.

Interestingly, functionalized rGO can be made not only by functionalization of rGO but also by reduction of functionalized GO. The latter strategy is preferred because GO has more diverse feasible reactions. GO is an excellent template for manipulating the functionality of graphene owing to its unique chemical structure composed of small sp^2 domains with sp^3 carbon domains and oxygen functional groups. However, randomly oriented oxygen groups make it hard to control selective chemical modification, leading to minimal changes in electrical and optical properties. Table 4 indicates methodology for controlling the functionality of GO. For each oxygen functional group, GO is modified by a different route of amidation and esterification. First, the carboxylic group requires a coupling reagent such as thionyl chloride ($SOCl_2$), 1-ethyl-3-(3-dimethylaminopropyl)-carbodiimide (EDC), *N,N'*-dicyclohexyl-carbodiimide (DCC), or 2-(7-aza-1H-benzotriazole-1-yl)-1,1,3,3-tetramethyluronium hexafluorophosphate (HATU) to add a nucleophilic species for amidation or esterification. Tang et al. presented covalently functionalized GO with 2-amino-4,6-didodecylamino-1,3,5-triazine (ADDT). The presence of ADDT changed the polarity of GO and led to homogenous dispersion in non-polar solvents¹⁵⁸. In addition, covalent bonding between GO and chromophores such as oligothiophene, P3HT, porphyrins, phthalocyanines, azobenzene, have been attempted in order to change optical properties (fluorescence intensity, lifetime, extinction coefficients) and dispersibility. GO can be also grafted to a polymer, where its property is affected by dispersibility, mechanical strengthening, and morphologic characteristics of

the polymer, and by conductivity, chemical reactivity, and mechanical reinforcement from graphene. The aim of polymer grafted GO is mostly to enhance mechanical properties, dispersibility, and biocompatibility. In particular, polyethylene-imine (PEI)/polyethylene glycol (PEG)-modified GO has been comprehensively investigated for biological applications because PEI/PEG is a biocompatible superhydrophilic polymer. PEI/PEG modified graphene allows adsorption of negatively charged biomolecules via electrostatic interaction, leading to low cytotoxicity and a fluorescence quenching effect¹⁵⁹.

3. Hybrid electrodes with NW or Graphene

Hybrid composites have been developed with a combination of different nanomaterials on/in various polymers to overcome the disadvantages of each individual material. Here, we will first compare the intrinsic mechanical and electrical properties of metal NW and graphene and then we will look into hybrid composites that overcome the mechanical and electrical limitations of NW and graphene.

3.1. Mechanical property modulation

AgNW has been intensively used in both stretchable and flexible electrodes. Structural defects, size, and adhesion of NW affect flexibility, which is related to the yield strength of the composite. Structural defects and size affect the intrinsic mechanical stability of NW, whereas adhesion determines the macroscopic mechanical stability of the network¹⁶⁰. NW with a small number of defects and smaller diameter exhibits a large young's modulus, high yield strength, and high ultimate tensile strength due to the concentrated stress on the defect site and stiffening size effect in the young's modules, respectively^{161,162}. The degree of adhesion of NW on substrate, however, determines the mechanical stability of composite more dominantly, because a soft electrode with nanomaterials has a very large substrate thickness (approximately $\sim 100 \mu\text{m}$) compared with nanomaterial film ($<100 \text{ nm}$). When NWs adhere loosely on a substrate, the NW network peels off or slides by application of friction or adhesive tape directly on the NW. Tightly linked NW with a stretchable matrix has an excellent ability to follow the substrate flexibility and NW movement relies on the strain history remaining on the substrate, leading to reversible stretchability within the range defined by the first strain. Interestingly, a physically welded NW network shows a "meandering" mesh-like mechanical tendency, which is reported to be stretchable up to 100% for a biaxial strain¹⁶³, unlike the sliding phenomenon of non-welded NW. One study showed clear differences in mechanical stability before and after welding⁷². Non-welded Ag NWs showed huge sheet resistance fluctuation, especially in the first 1-3 cycles, but there was no significant change in sheet resistance even after 10,000 bending cycles following the welding process. Another mechanical disadvantage of NW is its weakness to rubbing or scraping, although this can be reduced by encapsulation. Our group has developed an encapsulation system with multilayered graphene oxide and polydiallyldimethylammonium chloride (GO-PDDA) that can

prevent rubbing of the AgNW network¹⁶⁴. Tribological tests at the micro- and nanoscale demonstrate that (GO-PDDA) layers can effectively protect AgNWs on the substrate from external friction to enhance a sliding phenomenon of GO, which affects the lower subsurface maximum von Mises stress. As a result, (GO-PDDA)/AgNW/PET films can sustain a longer or larger force than AgNW/PET film.

Theoretically, the extraordinary mechanical stability of graphene makes graphene-based soft electrodes a fascinating option. Graphene is highly unique because it demonstrates high flexibility and brittleness at the same time. It also shows high mechanical stability, such as a breaking strength of 40 N/m and Young's modulus of around 1.0 TPa, and it can be stretchable by as much as 20%¹⁶⁵. However, grain boundary and defects dramatically decrease the original mechanical strength (150 GPa fracture strength)¹⁶⁶. Young Hee Lee's group observed crack creation and propagation depending on applied strain using optical microscopy¹⁶⁷. More cracks were created as the radius of curvature decreased and the crack was propagated along the strain direction and terminated at the graphene grain boundaries. The crack length is more important than the crack shape in determining the tensile strength of defective carbon material¹⁶⁸. Finally, defective graphene induces a dramatic degradation of electrical performance during stretching. Thus, several strategies to overcome defect-induced low fracture strength have been developed. The capability to endure large strains can be provided by using pre-strained substrate or by 3D graphene formation. Reversible control of crumpling and unfolding of graphene is demonstrated using a biaxially pre-stretched substrate because strongly adhered graphene pulls the delaminated graphene region, whereas uniaxially relaxed graphene electrodes lead to wrinkling and delaminated buckles¹⁶⁹. Another group reported a direct 3D graphene synthesis method. Graphene grown on wavy Cu foil presents approximately 60% transmittance (at 550 nm) and stretchability up to 40% strain on PDMS¹⁷⁰ and 3D graphene generated by direct graphene growth on Ni foam also exhibits high electrical conductivity of 10 S/cm and a maximum stain of 50%¹⁷¹.

A hybrid composite with enhanced mechanical properties is derived by different strategies for NW or graphene. Even though NW gives high stretchability by percolation theory, the low intrinsic mechanical strength (4.8 GPa fracture strength for Ag, 2-8 GPa for Au¹⁶⁰), low adhesion with other materials, and lack of functionalization methods hamper production of a highly stretchable NW-based composite. A mix of NW and another conductive nanomaterial is an alternative way to overcome these limitations of NW. Most hybrid systems with NW are related to enhancing the adhesion between NW and polymer.

We compare the mechanical stability of various AgNW hybrid composites in Figure 12c and f. AgNW-CNT composite was intended to enhance the stretchability of the AgNW network¹⁷². SWCNT have a more elastic nature and better interaction with polymer, leading to mechanical stability greater than 460%. In addition, CNTs fill the space between

nanowires and thus reduce deformation of the NW network and reduce resistance, providing local electron transport paths. In other studies, a polydopamine modified elastomer was used for a stretchable NW transparent conductive film. Polydopamine, which is present in the adhesive threads of mussels, plays an important role in bonding AgNW with polymer substrate. The resulting film exhibits 80% transmittance with an average sheet resistance of $\sim 35 \Omega/\text{sq}$ and maintains up to 20% mechanical elongation. Unlike NW, integration of graphene with other materials is mostly focused on electronic property modulation because of its good adhesion with polymer but relatively low conductivity. Graphene strongly interacts with polymer via van der Waals interaction, and further interaction can be generated by controlling the functionality of graphene. Polymer-conjugated graphene combines the physicochemical properties of both graphene and polymer. Polyanilines¹⁷³, polypyrroles¹⁷⁴, polythiophene¹⁷⁵, poly(phenylene vinylene)¹⁷⁶, and polyfluorenes¹⁷⁷ can be attached to graphene either covalently or non-covalently. Polymer-conjugated graphene produces well-dispersed single-layer graphene nanosheets in the polymer matrix, leading to enhanced mechanical and electrical properties of graphene-polymer composites.

3.2. Electrical property of soft electrode

NW seems to be a better electrode candidate than graphene derivatives because of its high carrier concentration and mobility. Takehiro Tokuno et al. reported that an AgNW network with CNT increases film conductivity to enlarge electrical paths and reduce the contact resistance between NW¹⁷⁸. However, graphene may be more suitable with respect to the tunability of electronic properties. A simple way to control the work function of graphene is by chemical doping. An rGO electrode with hydrazine reduction and subsequent thermal reduction has been reported as a n-doped graphene electrode and exhibits good conductivity with high transmittance and high electroluminescence efficiency ($17000 \text{ cd}/\text{cm}^2$) at flexible PLED due to the reduced barrier for electron injection¹⁷⁹. The graphene derivatives demonstrate slightly different work function. With hydrazine-treated reduction, CVD graphene shows 4.94 eV whereas rGO shows approximately 4.7 eV. The work function of rGO is different depending on the reduction type. The initial state of GO exhibits HOMO at 5.0 eV and LUMO at 3.5 eV, and after reduction the work function of rGO is determined by existing oxygen functional groups¹⁸⁰. A large oxygen content ratio produces a higher work function. Especially, carbonyl-rich rGO presents a higher work function (~ 5.2 eV for rGO with 12% oxygen remaining) than hydroxyl-rich rGO (~ 5.1 eV for rGO with 12% oxygen remaining). Graphene can also be modulated by the underlying or overlying material. Boseok Kang et al. observed that a self-assembled monolayer on the substrate controls the work function of the graphene above it¹⁸¹. A NH_2 (aminopropyl triethoxysilane, APTS) modified surface shows graphene N doping behaviour ($\phi=4.6$ eV), whereas direct functionalized rGO showed a shifted work function ($\phi=4.31$) with the same APTS molecule. Interestingly, some types of

doped rGO/graphene undergo both work function changes and decreased resistance, but others exhibit the desired work function shift and increased resistance. In general, acid treatment and metal insertion using a metal precursor solution dramatically decrease the resistance of graphene derivatives. However, rGO, graphene, and doped graphene still have much lower conductivity than metal NW therefore graphene integrated with other materials has been proposed as an alternative method to enhance conductivity as well as to control work function of graphene-based electrodes. Most hybrid composites with graphene for soft electrodes are a combination of graphene-polymer-metal component, such as NP and NW. Physisorbed metals such as Al, Cu, Ag and Pt, which have weak interactions with graphene, affect the Fermi level of graphene shifts without perturbing the graphene band structure because of the work function differences¹⁸². Thus, insertion of such weak interacting metals into graphene is widely exploited. Especially, AuCl_3 with nitromethane-doped graphene shows p-type behaviour and the highest decrement in resistance among other doping methods shown in Figure 12d,e¹⁸³. Graphene with metal ion insertion or metal NP is not comparable to a metal-based soft electrode because numerous NP-NP junctions generate high contact resistance and charge carrier scattering. Thus, graphene with 1D metal NW has recently been intensively researched. A 1D material is able to cross-link different domains that are divided by grain boundary. AgNW provides new conductive pathways for charge carriers in polycrystalline monolayer graphene, resulting in a high conductivity. This co-percolating conduction of the NW network and graphene domain mutually helps the transport bottleneck of each material. The NW percolating networks reconfigure with strain and bridge the cracks in the graphene film to maintain the electrical conductivity¹⁸⁴. Consequently, graphene with AgNW electrodes show very low resistance of around $22 \Omega/\text{sq}$ and n-type doping behaviour due to the lower work function of Ag (4.3 eV). Jang-Ung Park's group also studied a transparent conductive film using graphene with AgNWs. The film shows not only low sheet resistance ($33 \Omega/\text{sq}$) with high transmittance (94% in visible range), but also high flexibility (sustain 27% strain) and stretchability (100% in tensile strain)²⁹⁰. High mechanical strength is governed by AgNW linker between neighbouring graphene domains, leading to enable a stretchable transparent electrode with in plane configuration as well as out-of-plane configuration^{291,292}. Furthermore, graphene protects chemical and radiation damage of NW in graphene/NW hybrid structure. In many applications NW suffer from oxidation during both manufacturing process and operation. However, hybrid structure prevent in any oxidant component, even light²⁹⁰. Same group demonstrate good oxidation resistant under 85% in humidity, 85 °C and successfully produce wearable soft contact lenses. As a result, Chemical stability and mechanical stability are governed by the graphene and high conductivity is determined by the metal component. In addition, graphene fibre with AgNW was also suggested and the amount of NW determines the electrical conductivity and mechanical compliance of such fibres¹⁸⁵. Similarly, graphene-metal

nanotroughs hybrid system can effectively enhance nearby active layer is essential to reduce the energy barrier for

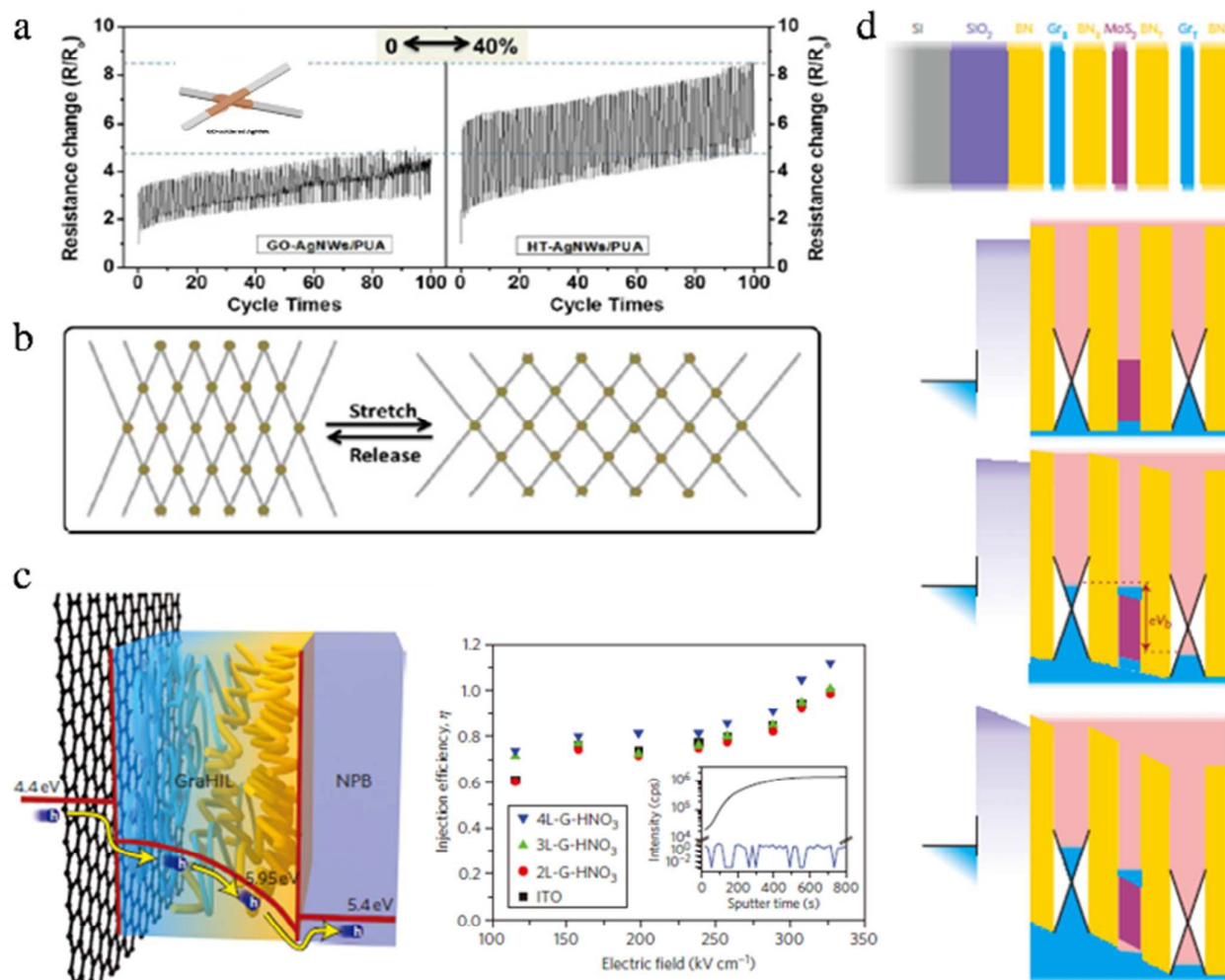


Fig. 13 a) Resistance changes at the stretching (40% strain) and releasing process for Go soldered AgNW network and thermal fused AgNW composite. b) Schematic configuration of stretching behaviour of Go soldered AgNW network¹⁹⁰. c) OLED device structure with graphene hole injection layer and performance as a function of the number of graphene layers¹⁹¹. d) Representative band diagram of an ultrathin heterostructure LED device¹⁹².

electronic properties by a complementary strategy¹⁸⁶.

4. Applications

4.1. Optoelectronic devices

4.1.1. Layered structure devices: LEDs and OPVs. Light emitting diodes (LED) and organic photovoltaics (OPV) function through opposite mechanisms; LEDs generate light from electricity, whereas solar cells create electricity from light. To convert electricity to light or light to electricity, the electron and hole should subsequently move through the layered structure with minimum recombination. Thus, two electrodes (cathode and anode) play an important role in collecting or injecting carriers in the desired direction. Transparent conductive film is generally placed in the electrode that generates or injects the hole carrier. For high efficiency, an ohmic contact between the transparent conductive film and

carrier transport and carrier recombination. The work function of the electrode and the adjacent layer determines whether there is ohmic contact or not. For efficient hole transport the HOMO level of active material and one electrode should be matched and for efficient electrons transport the LUMO level of active material and opposite electrode should be matched¹⁸⁷. Additionally, absorption in the visible region of the electrode material is important because light must pass through to the active material or out of the device. In general, a LED with an AgNW electrode shows high power efficiency because of the large local current density around the AgNW and high light extraction efficiency due to the light scattering effect of AgNW. An embedded AgNW electrode can be used for a flexible LED to reduce surface roughness⁶⁶. Because of the 1D shape, AgNW shows large surface roughness, which can trigger electrical shorting or disproportional carrier flow related to leakage current. Most OPV devices use an AgNW electrode, and therefore have an additional PEDOT:PSS layer

as both a smooth layer and hole injection layer (HIL); however, a PEDOT:PSS that is too thick reduces average current density. Polyvinyl alcohol (PVA) can be used to reduce the surface roughness of NW percolation networks by an embedded technique. The AgNW/PEDOT:PSS/NPB/Alq3/LiF/Al device shows higher power efficiency with a significantly reduced surface roughness (to 1–5 nm) and thermal and chemical stability compared to ITO-based organic LED. However, the embedded technique commonly suffers from poor hole injection. Other studies have demonstrated improved organic LEDs using a simple plasma treatment to remove the thin polymer overlayer on the NW network¹⁸⁸.

Interestingly, Qibing Pei's group fabricated a stretchable LED device with AgNW composite¹⁸⁹. The AgNW and poly(urethane acrylate) (PUA) composite showed sheet resistance of 10 Ω /sq and transmittance of 80% at 550 nm. The stretchability of film depicts the resistance change to 235 Ω /sq at 100% strain and the associated LED sustained 120% uniaxial strain for light on. To improve mechanical sustainability, the same group applied a GO soldered AgNW transparent electrode on polymer LED (Figure 13a,b)¹⁹⁰. Oxygen functional groups on GO effectively interact with the polymer, narrowing the AgNW junction. Accordingly, the AgNW network is wrapped with GO, which increases conductivity and minimizes disjuncting or sliding of AgNW when the strain is applied.

Graphene is another fascinating candidate in the field of flexible LEDs because of its atomically thin and flat nature. The low conductivity and relatively low work function (~4.4 eV) of graphene hamper luminous power efficiency by high operation voltage, and current efficiency is reduced by a high injection barrier in flexible electronics with graphene electrodes. One group modulated the electronic properties of graphene by doping with nitric acid AuCl₃ (Figure 13c)¹⁹¹. Doped graphene presents surface work function of up to 5.95 eV and reduced sheet resistance of 30 Ω /sq. A LED device with p-type doped 4-layer graphene gives a high luminance of approximately 30.2 cd/A, current efficiency of 98.1 cd/A, and luminous efficiency of 37.2 lm/W and 102.7 lm/W in flexible fluorescent and phosphorescent LEDs respectively. Interestingly, the Novoselov group demonstrated a novel type of flexible LED using only 2D, nanosheets (Figure 13d)¹⁹². Quantum wells are considered an active layer in the ultrathin vertical heterostructure LED. Single quantum wells (SQW) are composed of hBN/GrB/2hBN/WS₂/2hBN/GrT/hBN and multiple quantum wells (MQW) are composed of hBN/GrB/2hBN/MoS₂/2hBN/MoS₂/2hBN/MoS₂/2hBN/MoS₂/2hBN/GrT/hBN. hBN is used for a passivation layer that prevents spontaneous carrier transport in an undesired direction and to enhance the probability of photon generation for injected carriers. Accordingly, MQW, rather than SQW, increase quantum efficiency to increase the overall thickness of the tunnel barrier. This system allows higher current densities, reduced contact resistance, and luminescence uniformity. Emitting light frequency can be tuned by the appropriate choice of 2D semiconductors and the final structure gives an extrinsic quantum efficiency of nearly 10% within 10–40 atomic thickness.

The issues concerning AgNW-based OPV and graphene-based OPV are similar to those of LED with AgNW and graphene electrodes. Reducing surface roughness and modulating the state of the junction are dominant issues for AgNW-based OPV. Surface roughness can be reduced by a two-step process. ZnO is deposited on an AgNW network and roll-to-roll pressing is subsequently applied on the film¹⁹³. OPV using a compacted AgNW electrode shows good performance in both single cells with lower band gap polymer and tandem solar cells because of the flat and well-conjugated AgNW network with a low resistance (10–20 Ω /sq) and high transmittance. Use of AgNW with PEDOT:PSS, which is a similar strategy to the AgNW-based LED, was also attempted¹⁹⁴. On the other hand, junction welding can be prepared by biocompatible polymer sol-gel transition¹⁹⁵. PET is modified by alginate and then AgNW is deposited by bar coating. After CaCl₂ is exposed on the film, the stabilizer on AgNW is removed and metallic Ca²⁺ ion reacts with the alginate, leading to gel formation. The tightly bound alginate gel at the AgNW junction is water resistant and the P3HT polymer solar cell with this flexible and stable electrode has a power conversion efficiency of 2.44%.

Graphene has been used as both a cathode and anode in solar cells. The resistance of the electrode itself and the parallel resistance of the device are important to improve the efficiency of graphene-based OPV. One study reported OPV with modified single-layer graphene as a cathode¹⁹⁶. The device structure was ITO/PEDOT/CuPC/C60/TPBi/graphene. Single-layer graphene undergoes contact doping by the TPBi molecule with a successful shift in work function, leading to a power conversion efficiency of 0.41% in OPV (compared with a power conversion efficiency of 0.24% when graphene is used as an anode with the same device configuration). Other studies observed improved power conversion efficiency above 1.71% to modulate the work function of a graphene anode¹⁵⁶. When pyrene buanoic acid succidimidyl ester is physisorbed on a layered graphene the work function of the electrode changes from 4.2 eV to 4.7 eV. The graphene/PEDOT:PSS/P3HT:PCBM/LiF/Al structure demonstrates ~55.2% of the power conversion efficiency of a handmade OPV with an ITO electrode (ITO/PEDOT:PSS/P3HT:PCBM/LiF/Al). Yu Wang et al. also developed OPV using a layer-by-layer stacked graphene anode, and modulated its work function from 4.36 eV to 5.47 eV with acid doping and MoO₃ doping¹⁹⁷. In particular, the hydroxyl groups of MoO₃ strongly interact with PEDOT:PSS therefore the uniformity of the film is enhanced during the coating process. As a result, interface engineered graphene-based OPV yields 83.3% of the power conversion efficiency of ITO. To date, the conductivity of graphene is still not high enough, and should be enhanced by more effective doping or by interface control in the future.

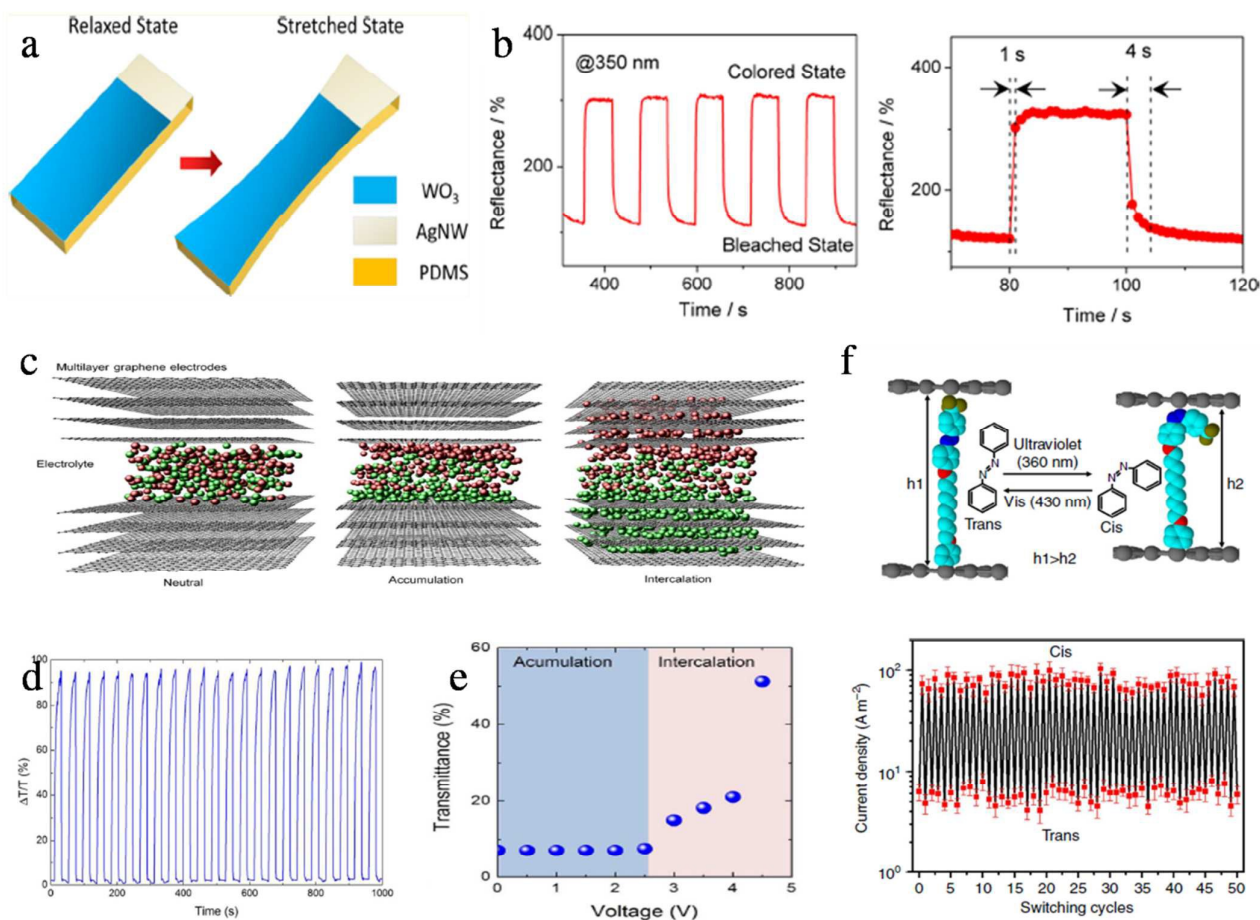
4.1.2. Touch screens. ITO has some drawbacks with respect to flexible touch screen devices, for example, brittleness, relatively high index of refraction ($n=2.0$), poor transparency in the near infrared (NIR) region, restrictive deposition conditions, and low chemical stability (in basic and acidic conditions). Graphene and AgNW have different strengths and weaknesses as a transparent electrode for touch screens.

Graphene exhibits high chemical stability, good transparency in the NIR region, and high flexibility, but relatively low conductivity and a high index of refraction ($n=3.0$)¹⁹⁸. On the other hand, AgNW presents a low refractive index of around 1.5 ($d=750$ nm, $l=45$ μ m), good transparency in the NIR region, and good conductivity with high flexibility, but poor chemical stability and high light scattering. In other words, the two materials can be applied to different types of touch screen. A touch screen is fabricated by resistive, capacitive, surface acoustic wave, surface capacitance, or projected capacitance methods. Among these, resistive method and capacitive methods are the most commonly used. Flexible transparent CVD grown graphene and CNT electrodes are applied to touch screen panels by the resistive rather than the capacitive methods due to the relatively high sheet resistance. The resistive method determines the position of a finger by pressure-induced current changes such that relatively high resistance on the electrode does not significantly affect current changes dependent on touching. The capacitive method perceives this by capacitance changes; the finger changes total capacitance as a result of integration of additional impedance in the circuit, which is called capacitive

coupling¹⁹⁹. For instance, ByungHee Hong's group fabricated a large area graphene electrode using a roll-to-roll process to make a resistive touch panel¹⁰⁸. The graphene-based panel is sustained until 6% strain, whereas ITO easily breaks under 2–3% strain. Although rGO has relatively low conductivity compared to CVD graphene, flexible touch screens with rGO have been successfully demonstrated¹¹⁷. A uniform graphene film is produced by mayrod coating, leading to a standard deviation of resistance of 3.7–9.8% over 100 cm². The final device shows 1.4% x-axis linearity and 1.2% y-axis linearity, which is comparable to that of conventional ITO-based touch screens.

In addition, a NW-based touch panel was proposed using a planary AgNW network with PEDOT:PSS²⁰⁰. Previously, many researchers have deposited PEDOT:PSS on the underlying AgNW network. During the coating process, PEDOT:PSS solution tends to destroy and sweep away AgNW. To overcome this issue, PEDOT:PSS can be selectively deposited on the junction area of the AgNW network, rather than on all regions. Additionally, isopropyl alcohol is added to the PEDOT:PSS solution to control the surface tension of PEDOT:PSS and the solvent evaporation rate. The capillary

Fig. 14 a) Illustration of stretchable electrochromic device with AgNW electrode and b) its switching behaviour depending on reflectance changes²⁰³. c) Mechanism of graphene based electrochromic device. Under high bias voltage, graphene shows significant optical changes due to intercalation of electrolyte. d–e) Switching behaviour of graphene based devices as a function of time (d) and voltage (e)²⁰¹. f) Description of azo-based photoswitching molecular electronics and its on/off characteristic²⁰⁴.



force assists the nanosoldering behaviour of PEDOT:PSS and leads to enhanced contact resistance on the junction and adhesion to the substrate.

4.1.3. Electrochromic/Photo-switch devices.

In electro-

AgNW has been researched as an electrode in flexible electrochromic devices, despite the disadvantage of easy oxidation by electrolytes or in an acid/base environment. Chaoyi Yan proposed an inorganic electrochromic device with

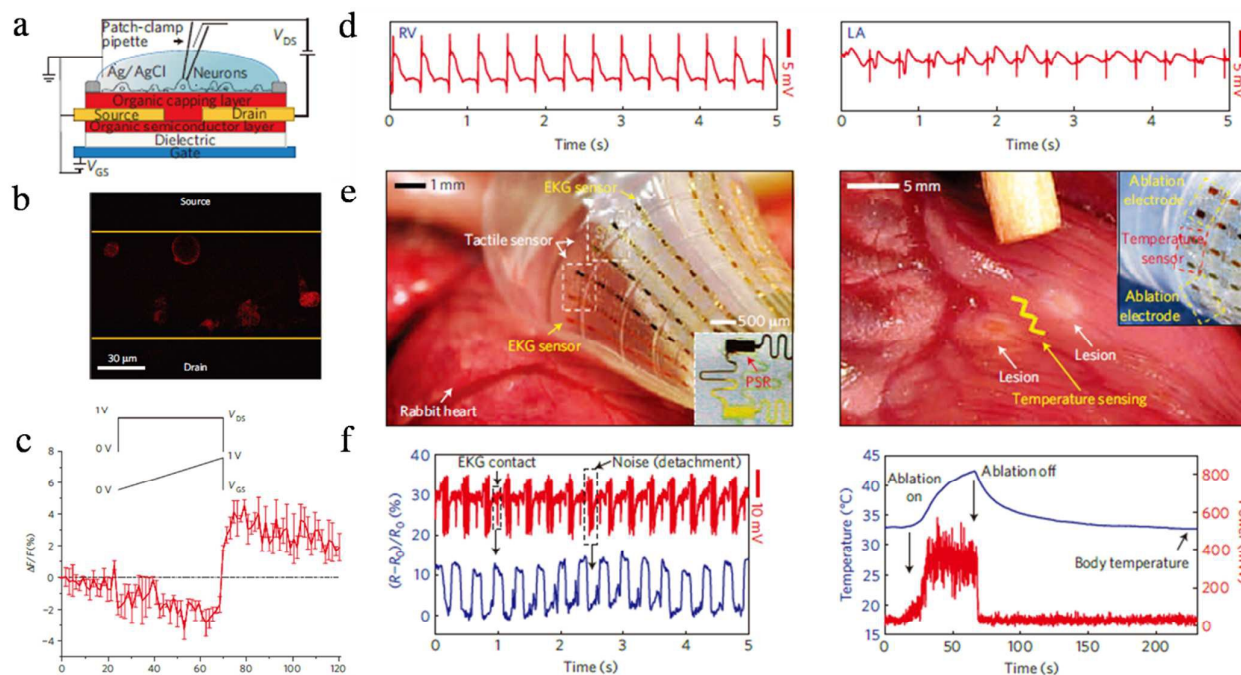


Fig. 15 a) Device structure of OFET for electrophysiological recordings. b) Laser scanning confocal microscopy image of neuron growth on organic capping layer and c) fluorescence intensity changes as a function of time after bias voltage²¹⁹. d) Cardiac electrophysiological signal map of right ventricle and left atrium surfaces. Signal-to-noise ratios are approximately 60 dB e) Optical image of a real operation process on the heart. f) Electrical signal correction with mechanical contact and temperature monitoring before, during, and after RF ablation²²⁰.

chromic devices, the colour of electrochromic material between two electrode changes reversibly as a result of transported electrons or liquid/polymeric ion movement at the applied voltage. Thus, we can observe colour changes through the side of transparent electrode. Polat et al. suggested a novel type of flexible electrochromic device using multilayer graphene as both electrode and electrochromic material (Figure 14c-e)²⁰¹. Graphene has high contrast optical modulation over a broad spectrum, and significant doping induced by ionic movement at distributed electric field can change its optical behaviour. The transmittance of graphene increases to 55% at 900 nm when 5 V is applied, whereas that of graphene decreases by 8% with broad wavelength at 0 V. The gate-tunable optical properties of graphene originate from blocking interband transition of the graphene layers via electrostatic doping. Not only the optical properties, but also high electrical conductivity and good flexibility, allow graphene-based electrochromics with excellent performance. One group demonstrated an electrochromic device using ionic liquid functionalized graphene²⁰². The electrochemical and optical properties of PEDOT, which is an active material, are changed depending on the applied voltage. Without applied voltage, PEDOT maintains a fully oxidized state and shows transmissive colour in the visible region. At -1.5V, Li^+ and ClO_4^- on graphene move toward PEDOT and PEDOT is altered to a reduced state, resulting in a blackish-gray colour. In addition,

an AgNW electrode in which AgNW is embedded on PDMS and acts as a protecting layer (Figure 14a)²⁰³. Thus, embedded AgNWs in this device can survive in a chemically and mechanically harsh environment during operation. They authors observed fast coloration (-1.8V) and bleaching (-0.5V) processes even in a stretched state (50% strain).

Graphene and AgNW-based transparent electrodes can be used in various photoswitch devices such as molecular electronics or photodetectors. Because of its atomically flat surface graphene is dominantly used in molecular electronics, not only for photoswitching but also for voltage-derived devices. Molecular electronic devices have been investigated in terms of understanding molecular charge transport mechanisms and potential device applications. The main issues in this field are device yield and the leakage current. Direct metal deposition on the molecules easily causes filamentary paths and damage to the molecules, resulting in electrical short circuits and unexpected current voltage characteristics. To deal with these issues, our group explored graphene-graphene electrodes for molecular electronics (Figure 14f)²⁰⁴. A chemically inactive and flexible graphene electrode does not affect the state of assembly of molecules or their degradation. Only electronic coupling between graphene and molecules occurs and further covalent bonding is able to reduce the contact resistance of the device. In this system, a molecular monolayer between graphene provides a similar molecular

length-dependent J-V characteristic to that of previously reported molecular electronic system. The same device with a photoactive molecule can serve as a photoswitching molecular electronic because of the high transparency of graphene electrodes. The graphene-aryl azo benzene monolayer graphene junction shows current changes with UV/VIS irradiation. Another type of photoresponse device called a photodetector has been developed using graphene and AgNW. In this device photoactive copper hexadecafluorophthalocyanine between rGO gap electrodes provides a photo-response^{205,206}. A clean and highly conductive rGO electrode is fabricated by applying an electric current on GO film and deposition of copper hexadecafluorophthalocyanine between two rGO electrodes. A final rGO-based photodetector gives a switching ratio of approximately 20 before and after light on. Other studies report AgNW-based photodetectors formed with Zn₂SnO₄ active NW channel in which Zn₂SnO₄ NW is sandwiched by two AgNW electrodes²⁰⁶. Two AgNW electrodes are patterned in a parallel direction, whereas Zn₂SnO₄ NW is in the cross direction. The device was examined with 5 V and on and off UV light and exhibited response time below 0.8 s, a fast reset time of 3 s, and high stretchability up to 50%.

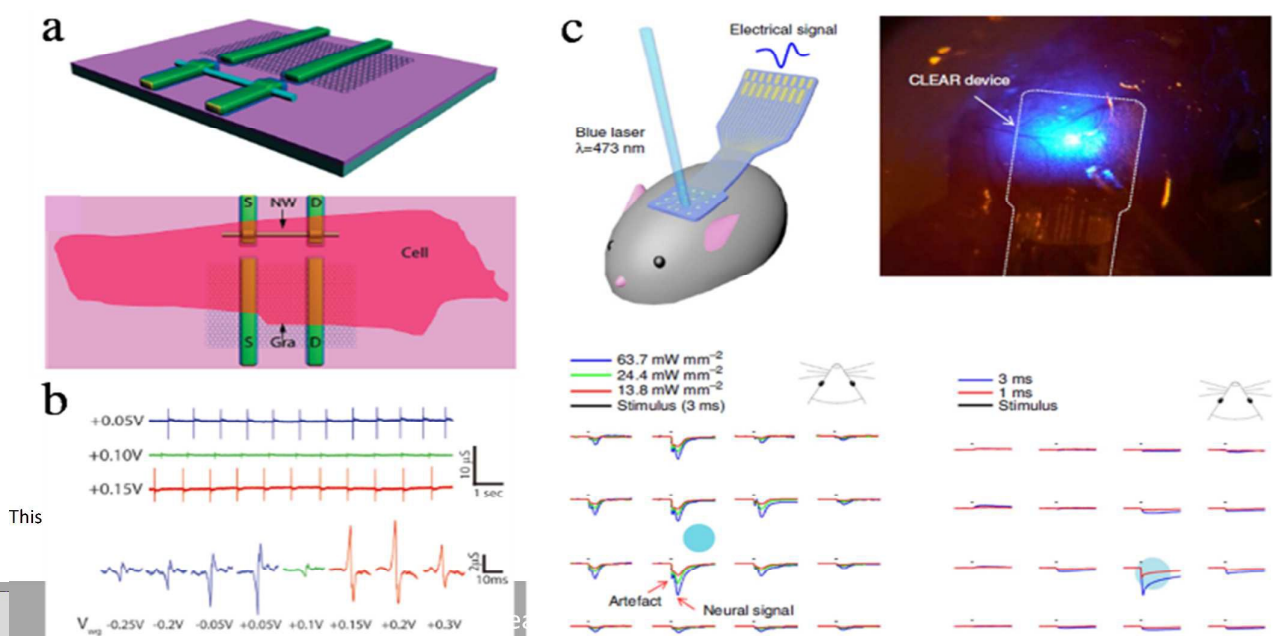
4.2. Biointegrated devices

Improvements in stretchable and flexible electrodes appear to offer significant opportunities for emerging human interface applications, such as conformal biosensors, measurement of electrophysiological signals, and delivery of advanced therapies. Electrodes on biointegrated devices should be non-toxic and stable in an aqueous environment. Up to now, new structural layout strategies have been predominantly employed in flexible bioelectronics. For example, the Lieber group propose high-yield syringe-injectable electronics using a polymer-encapsulated metal mesh²⁰⁷. The mechanical properties of the free standing mesh electronics are determined by the width of the mesh, the angle of tilt, and the inner diameter of the syringe. Tilted metal mesh results in enhanced free standing of the electrode during injection and

adhesion to neurons because a tilted shape reduces transverse bending stiffness. Recently, nanodimensional materials have been applied in numerous biological fields due to their unique properties such as high flexibility, photoluminescence, and cell penetration ability. In particular, graphene, a naturally occurring carbon material, has attracted great interest because of its high conductivity and high transparency, in addition to its environmentally and biologically friendly nature^{208,209}. Moreover, AgNW has been exploited as a sensitive conductor because of the unique electronic properties and 1D shape of NW. In this chapter, we briefly introduce the current status of each bio-integrated device and present some examples of the use of AgNW and graphene electrodes.

4.2.1. Biosensors. High surface area, good electrical conductivity, chemical and electrochemical stability, and acceptable biocompatibility make graphene fascinating for application in the bioanalytical area of electrode design. Recently, many studies on graphene and its derivatives (GO, rGO, and multilayer graphene) in enzyme-based biosensors have been published. Graphene has been integrated on common biosensor systems with various enzymes and proteins such as cytochrome *c*²¹⁰, horseradish peroxidase²¹¹, alcohol dehydrogenase²¹², acetylcholinesterase²¹³, tyrosinase²¹⁴, glucose oxidase²¹⁵, and hemoglobin²¹⁶ to detect analytes such as glucose, H₂O₂, O₂, phenolic pollutants, organophosphates, catechol, ethanol, NADH, and nitric oxide. There are many issues related to graphene-based enzyme biosensors: good operational and storage stability, enzyme loading capacity, high sensitivity, selectivity, reproducibility, and the maintenance of an efficient link between the sensing molecule and a transduction component. M. Zhang et al. demonstrated a graphene solution-gated transistor for dopamine detection in which electro-oxidation of dopamine modulates the degree of gating on the transistor²¹⁷. A higher amount of dopamine increases the effective gate voltage applied on the transistor, leading to an increase in drain current. As a result, the detection limit of this device is decreased to 1 nM, compared

Fig. 16 a) Schematic illustrations of chip design highlighting the morphological differences between components (upper) and the relative size of cardiomyocytes (lower). b) Signal detection depending on water gate voltage. The action potential is clearly obtained²²². c) Operation scheme and photograph of neural stimulation by light sources. Action potential is successfully measured by laser stimulation with different power and post-mortem signal indicates the spontaneous disappearance of the light-driven action potential in optogenetic device²²³.



with 1 mM for the previous dopamine sensor, mainly because the weak π - π interaction between dopamine and graphene alters electrical changes in this system. In addition, AgNWs have been used as glucose biosensors²¹⁸. AgNW with high electrical conductivity, high surface area, and small size provides direct electron transfer between the enzyme and the electrode. AgNW improves the electrocatalytic activity of the enzyme and enhances the detection limit to 50 μ M.

4.2.2. Electro signal recording/stimulation: Brain and Heart.

High-resolution interface devices enable us to observe unknown features in the human body. Penetrating electrodes and surface-contacting electrodes with high flexibility and good biocompatibility are used to detect neuro- or cardiosignals. Penetrating electrodes sometimes lead to damage of tissue or cells during electrical recording, whereas microelectronic arrays for surface-contacting electrodes suffer from size-dependent electrode impedance and weak interfacial adhesion between the electrode and the bio-material, resulting in low resolution and sensitivity. In a recent study, improving the flexibility of the device and modifying the electrode significantly enhanced the electrical resolution of biointegrated devices to meet both the biological and electrochemical requirements of interfacial interaction. For instance, the Muccini group invented a transparent organic cell stimulating and sensing transistor using N,N'-ditridecylperylene-3,4,9,10-tetracarboxylic diimide (P13) as a channel material (Figure 15a-c)²¹⁹. P13 facilitates cell arrangement and cell coupling with the electrode so that the device yields a high signal to noise ratio to stimulate and record a single cell in real time. Neurons become active at a threshold voltage of 26.3 mV. Depolarization and hyperpolarization of the neuron is examined with and without tetrodotoxin (TTX), which inhibits the positive spike of neurons. Neuron cells treated with TTX show a decrease in the number of detected events. In addition, the transparent nature of the material allows optical imaging of the neuron. Another interesting strategy to detect the biosignal is using a highly flexible substrate. Dae-Hyeong Kim et al. demonstrated use of a balloon catheter device to map cardiac electrophysiological signals (Figure 15d-f)²²⁰. Balloon-like electronics allows effective attachment of the electrode to organs, cells, and tissues by controlled inflation and lead to minimally invasive insertion. Cardiac electrophysiological studies using a tactile sensor or temperature sensor in a balloon-like device generate a high-quality electrical activation signal. In bioelectronics, conductive polymers have been widely explored as channel electrodes because of their biocompatibility, effective surface area, and low impedance at the interface. Functionalized conductive polymers with biomolecules, growth factors, and neurotransmitters increase the quality of the signal even more, leading to better stimulation and monitoring of the biological process. However, low resolution, high signal to noise ratio, low scalability (necessary for comprehensive mapping of brain activity), and

low interfacing ability with optical or drug delivery element prevent further application of conductive polymers²²¹.

There have been several attempts to apply graphene electrodes for these electrosignal recoding/stimulation devices. A graphene-based transistor is used to record cellular interface electrical signals in Figure 16a,b²²². Both the back gate and water gate modulate the electronic features of graphene in this system; in particular, the water gate offset value affects the sensitivity of the device. Finally, a graphene transistor with cardiomyocytes yields a high signal to noise due to a stable interface between the graphene transistor and cell. Furthermore, Zhenqiang Ma and co-workers have suggested optogenetic application on neuron cells with a graphene electrode array (Figure 16c)²²³. To date, a transparent microelectrocorticography device has yet to be applied in a real living body because of the toxicity and rigidity of ITO with respect to chronic implementation. However, graphene, which has broad-spectrum transparency and biocompatibility, facilitates development of a microelectrocorticography device. A graphene-based device and a pt-based device were implanted side-by-side in rats and mice. At the early stage after implantation, the initial tissue response led to a sharp increase in impedance on both devices. Soon after, the tissue response become stable and provided minor day-to-day fluctuations in the impedance changes. Compared to the pt-based device, the graphene-based device exhibited a higher baseline:signal recording ratio and a successfully evoked potential when the implanted electrode was stimulated. Both potential stimulation and light stimulation have been examined to test optogenetic behaviour. Graphene shows transmission of over 90% in the UV to IR region, therefore light can pass through into the targeting organ or tissues. Here, a blue laser is used to stimulate brain signals and ensure in vivo imaging of neurons in addition to light-driven stimulation.

4.2.3. Artificial Skin. Significant efforts to find novel active materials and new fabrication strategies have been devoted to the realization of smart textiles. The actuator, a kind of motor to replace or simulate muscle, is the one representative case. In the actuator, an active polymer changes its shape in response to an electric field or ion movement. When actuated by the electrical field, a dielectric elastomer, electrostrictive polymer, and liquid crystal elastomer typically comprise the active materials whereas when actuated by ions CNT, the conducting polymer, and ionic polymer-metal composite perform that function. To achieve a high performance, AgNW has been regarded a promising candidate because of its intrinsic properties as a soft material. In one study of a bifunctional actuator, bistable electroactive polymers (BSEPs) were combined with AgNW to support high actuation strain and Joule heating (Figure 17b)²²⁴. AgNW embedded in polymers endured external friction without loss of conductivity and resulted in 140% strain durability. Therefore, AgNW fulfils the role of a new compliant electrode for both electrically and

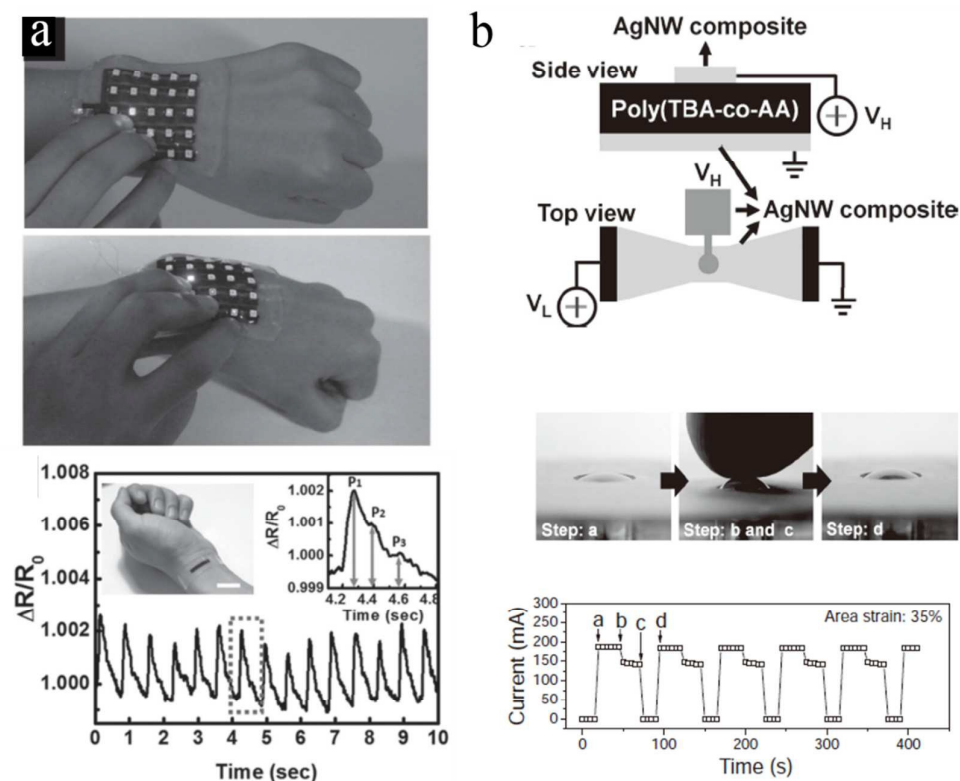


Fig. 17 a) Photograph and resistance changes of wearable strain sensors. Body movement is distinguished²²⁹. b) Schematic illustration of BSEP actuator (upper) and photographs showing the bistable characteristics of the actuator during 4 repetitive tests (step a: Joule heating, step b: applying electric field, step c: removing electric field and cooling down to RT, step d: 2nd Joule heating) (lower)²²⁹.

thermally induced actuation. Focusing on reversible sliding of the NW network, another group suggested an electrostatic actuator with AgNW electrode²²⁵. The sliding behaviour of the NW network brings high stretchability and also large variations in transmittance to the device. When a voltage is applied and the area of the network increases, densely connected NWs spread by sliding over each other. This phenomenon of NW can lead to actuation over a broader range of transparent states than among any other materials, which can be further evaluated by modulating the percolation. Actuators based on graphene electrodes have also been tested because of their high specific surface area, mechanical strength, and electrical conductivity, which might yield remarkable performances in combination with active materials. In electrochemical actuators, it is likely that the graphene sheet induces actuation through coulombic and quantum chemical-based expansion. Based on this explanation, Jiajie Liang et al. generated a much higher actuation strain (0.1%) by inserting Fe₃O₄ nanoparticles to prevent re-stacking of graphene flakes than with pristine graphene (0.06%)²²⁶.

Pressure sensors, another application related to artificial skin, have also been investigated. Operating through an opposite mechanism to the actuator, which deforms its shape in response to electrical changes, the pressure sensor displays electrical signals in response to the applied pressure. Although CuNW-PVA aerogel²²⁷ or AgNW²²⁸ can be used as an electrode in the pressure sensor, the aerogel type is preferred for its low cost and mild and simple processes despite a much lower

sensitivity (0.036 kPa⁻¹) than the AgNW-based device (5.54 kPa⁻¹). In the case of graphene, use of graphene foam, which has higher stretchability than 2D graphene sheets, results in constant resistance under external strain. Although low sensitivity is a weak point of a graphene foam-based sensor, one group achieved 20 times higher sensitivity by fragmentizing graphene foam and showed 70% stretchability with PDMS (Figure 17a)²²⁹.

A large contact area between graphene foam fragments contributes to an increased change in contact resistance under the applied strain, which can sensitively detect less than 1% of strain. Going beyond artificial skin, the Bao group introduced a self-healing conductive organometallic polymer into a pressure/strain sensor²³⁰. Nickel nanostructured microparticles are embedded in a supramolecular polymer host of weak hydrogen bonds that readily break under the strain. With these broken hydrogen bonds, which are known to associate and dissociate at room temperature (passive healing), the polymer chain is subsequently rearranged, wetted, and diffused on the fractured region because of its low T_g and finally accomplishes self-healing behaviour. A high conductivity of 40 S/cm can be obtained, and electrical properties are restored after a few seconds whereas mechanical properties are restored after few minutes. Finally, a tactile pressure sensor composed of stretchable and electrically self-healing electrode exhibits excellent pressure sensitivity²³¹. Piezoelectric PVDF fibres are sandwiched between conductive

PVA/rGO foam combined with PDMAA self-healing polymer and can detect a very light touch (0.02 kPa).

5. Perspectives for future work

Recent advances made with stretchable and flexible electronics provide new directions of research in various optoelectronic and biomedical fields. However, stretchable integrated electronics with layered structure systems still exhibit several unsolved issues. Especially, the complex fabrication process and transparency are major obstacles of these systems in spite of their stable device performance under high strain. New materials have received intensive attention due to their extraordinary electrical and mechanical properties. Investigations of stretchable soft electrode were carefully reviewed with an emphasis on mechanical and electrical properties depending on dimensionality of the nanomaterials. The new nanomaterials, 1D metal NW and 2D graphene derivatives, exhibit different intrinsic properties to those of the single materials and the collective behaviour of their network. In the case of metal NW, electrical, optical, and mechanical characters of NW rely highly on the percolation theory therefore the junction state is important. Generally speaking, low adhesion of NW tends to cause large contact resistance, high surface roughness, and high light scattering, which result in a low-quality electronic performance. Thus, for the metal NW, high adhesion on the substrate has become a key issue. On the other hand, graphene has huge charge carrier mobility because of p orbital Dirac fermions with zero effective mass and its physical properties can be modulated by specific surface chemistry. However, unlike theoretical single crystalline graphene, polycrystalline graphene and rGO show relatively low conductivity; this is one of the biggest drawbacks of graphene, although strategies to overcome low conductivity driven by grain boundary, defects, and oxygen functional groups are under development. In particular, a doping technique on graphene can be considered an effective method to modulate the work function and carrier density of graphene. Even though many technical improvements on AgNW and graphene have been demonstrated to enhance the performance of soft electronics, the use of each material alone still has its own intrinsic limitations. Consequently, hybrid electrodes have been developed as promising new candidates. A combination of different nanomaterials can exhibit sharply enhanced conductivity and mechanical stability. The limitations associated with the mechanical property of AgNW, which has high conductivity but a fragile nature, can be overcome by adding carbon allotropes and/or conductive polymer, which has high mechanical strength. Hence, graphene derivatives have been mixed with metal NP and/or NW to enhance their conductivity. The hybrid electrodes show huge improvements and have been successfully applied to many stretchable electronic applications.

In this report, we also attempt to offer some perspective on the best applications for each material or material composition. For example, graphene, which has an ultrathin transparent conductive layer, may be the most appropriate

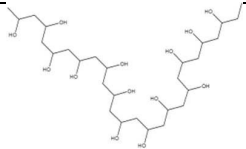
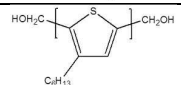
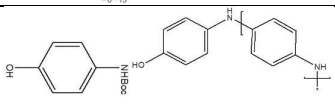
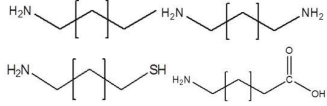
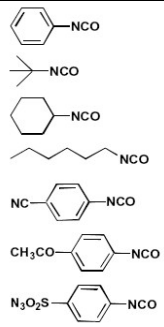
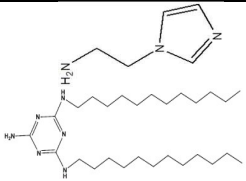
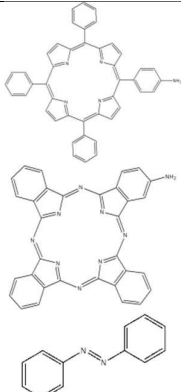
choice for molecular electronics using monolayer molecules whereas AgNW should be the best fit as a sensing material due to its high conductivity and high aspect ratio. Especially, graphene electrodes are attractive in many biomedical applications because of their high conductivity combined with biocompatibility. AgNWs and graphene flakes can serve many different and various purposes not only in optoelectronics, but also in biological applications, even though both graphene and AgNW have a huge potential to alter ITO on stretchable and flexible devices. Electrosignal recoding/stimulation, pressure sensors, and actuators for artificial skin have been demonstrated using graphene and/or AgNW. Some of these show outstanding performance while others need to be further developed. To overcome their limitation, in-depth discussions about the intrinsic properties of each material and modulation of signal to noise ratio, flexibility, adhesion, and stability are needed. It is highly expected that the extraordinary physical properties of nanomaterials for stretchable electrodes will lead to breakthroughs in new types of optoelectronics and biointegrated devices in the future.

Table 3 Chemical doping for graphene derivatives

Type	Material	condition	R	ϕ	Device	ref		
metal	Increase ϕ	Au	spin coating	500	5		234	
		Ir	spin coating	600	4.9			
		Mo	spin coating	720	4.8			
		Os	spin coating	700	4.68			
		Pd	spin coating	520	5			
		Rh	spin coating	620	5.14			
	Decrease ϕ	Au(OH) ₃	spincoating and annealing	820	4.6		235	
		Au ₂ S	spincoating and annealing	600	4.8			
		AuBr	spincoating and annealing	530	5			
		AuCl ₃	spincoating and annealing	300	4.9			
		NaCl		1350	3.7			236
		KCl		1370	3.76			
		CaCl ₂		1530	3.81			
MgCl ₂		1630	3.9					
organic	P-type	TFSA(CVD)	spin cast	129	-0.7eV*		237	
		F4-TCNQ			4.7		238	
		TCNQ(CVD)		629	5.13	solar cell	239	
		PDI(Hummer's)	ReG-PDI dispersion			photovoltaic	240	
		phosphonic acid(exfoliation)	spread-coating				241	
		fluoroalkyl				FET	242	
		nitrobenzen(exfoliation)	drop-coating			FET	243	
	n-type	MeO-DMBI(CVD)	spin-coated onto graphene sheets	767	3.46	FET	244	
		An-ch3(exfoliation)	drop-cast			FET	130	
		Na-NH ₂ (exfoliation)	drop-cast			FET		
		TPA(exfoliation)	drop-cast			FET		
		Ab-Br(exfoliation)	drop-cast			FET		
		hydrazine(CVD)	Immersion for 2 h	517		FET		245
		aniline(exfoliation)	drop-coating			FET	243	
		TTF(exfoliation)	drop-coating			I/V characteristics	246	
		Triazine				bandgab tuning	247	
		PyS(hummer's)	ReG-PyS dispersion	916		photovoltaic	240	
		VOPC(exfoliation)	thermally deposited				248	
		PTCDA	Deposition			Semiconductor	249	
		Polymer	PEDOT:PSS(exfoliation)	spin coating			DSSC	250
nafion(exfoliation)	coating		30k			250		
PANI(exfoliation)	mix&ultrasonication				supercapacitors	252		
PDDA(exfoliation)	PDDA Functionalized Graphene					253		

*is relative value compared to non doped graphene. - 0.7eV means work function increase by vacuum level.

Table 4. Chemical Reaction of GO

OH component	Activation agent & condition	Purpose	ref
	DCC, DMAP in DMSO	Mechanical property (tensile strength, Young's modulus)	254
	SOCl ₂ , 65°C, 24hr Triethylamine, THF, 36hrs	Charge transfer as electron donor for PV	255
	SOCl ₂ , reflux Pyridine/THF, reflux TFA/MC, hydrolysis Aniline, APS	Conductivity	256
Amino component	Activation agent & condition	Purpose	ref
<Active site : COOH>			
	SOCl ₂ , DMF, 70°C R-NH ₂ , 120°C	Dispersibility	257 , 258
	Isocyanate, DMF, 24hrs	Dispersibility	259
	COCl ₂ , 80°C, 18hrs (Aminopropyl)imidazole, 100°C, 18hrs SOCl ₂ , 70°C ADDT, 120°C	Dispersibility	260
	SOCl ₂ , 70°C, 24hrs Et ₃ N, DMF, 130°C, 72h	Optical property change Increment of Extinction coefficient	261

Nanoscale		Optoelectronic application	Review
	SOCl ₂ , 70°C, 24hrs Et ₃ N, MC, rt	Optoelectronic application	<u>262</u>
	3M NaOH, EDC, Sonication	Biocompatible Drug delivery	<u>263</u>
	CS in MES buffer EDC, NHS	Solubility Biocompatible Nano carrier	<u>264</u>
	H ₂ O, EDC, 24hrs	Low cytotoxicity Higher transfection efficiency	<u>265</u>
<Active site : epoxy>			
	Acyl chlorinated graphene oxide Et ₃ N, DMF, 130°C, 72h	Mechanical property (tensile strength, Young's modulus)	<u>266</u>
	IL-NH ₂ , KOH, water 65°C, reflux	dispersibility	<u>267</u>
	APTS, catalyst 1) Mechanical reinforce 2) Intermediate for further rxn		<u>268</u>

Acknowledgements

This work was supported by IBS-R011-D1

Notes and references

- 1 C. Yan, J. Wang, W. Kang, M. Cui, X. Wang, C. Y. Foo, K. J. Chee and P. S. Lee, *Advanced Materials*, 2014, **26**, 2022-2027.
- 2 A. R. Madaria, A. Kumar and C. W. Zhou, *Nanotechnology*, 2011, **22**.
- 3 D.-H. Kim, R. Ghaffari, N. Lu, S. Wang, S. P. Lee, H. Keum, R. D'Angelo, L. Klinker, Y. Su, C. Lu, Y.-S. Kim, A. Ameen, Y. Li, Y. Zhang, B. de Graff, Y.-Y. Hsu, Z. Liu, J. Ruskin, L. Xu, C. Lu, F. G. Omenetto, Y. Huang, M. Mansour, M. J. Slepian and J. A. Rogers, *Proceedings of the National Academy of Sciences*, 2012, **109**, 19910-19915.
- 4 Y. Meng, Y. Zhao, C. Hu, H. Cheng, Y. Hu, Z. Zhang, G. Shi and L. Qu, *Advanced Materials*, 2013, **25**, 2326-2331.
- 5 L. Gomez De Arco, Y. Zhang, C. W. Schlenker, K. Ryu, M. E. Thompson and C. Zhou, *ACS Nano*, 2010, **4**, 2865-2873.
- 6 N. Lu, Z. Suo and J. J. Vlassak, *Acta Materialia*, 2010, **58**, 1679-1687.
- 7 N. Lu, X. Wang, Z. Suo and J. Vlassak, *Journal of Materials Research*, 2009, **24**, 379-385.
- 8 A. Khaund and P. Nicholson, *J Mater Sci*, 1980, **15**, 177-187.
- 9 R. Morent, N. De Geyter, F. Axisa, N. De Smet, L. Gengembre, E. De Leersnyder, C. Leys, J. Vanfleteren, M. Rymarczyk-Machal, E. Schacht and E. Payen, *J Phys D Appl Phys*, 2007, **40**, 7392-7401.
- 10 D.-Y. Khang, H. Jiang, Y. Huang and J. A. Rogers, *Science*, 2006, **311**, 208-212.
- 11 D.-H. Kim, J. Xiao, J. Song, Y. Huang and J. A. Rogers, *Advanced Materials*, 2010, **22**, 2108-2124.
- 12 Y. Sun, W. M. Choi, H. Jiang, Y. Y. Huang and J. A. Rogers, *Nat Nano*, 2006, **1**, 201-207.
- 13 D.-H. Kim, N. Lu, R. Ma, Y.-S. Kim, R.-H. Kim, S. Wang, J. Wu, S. M. Won, H. Tao, A. Islam, K. J. Yu, T.-i. Kim, R. Chowdhury, M. Ying, L. Xu, M. Li, H.-J. Chung, H. Keum, M. McCormick, P. Liu, Y.-W. Zhang, F. G. Omenetto, Y. Huang, T. Coleman and J. A. Rogers, *Science*, 2011, **333**, 838-843.
- 14 P. Lee, J. Lee, H. Lee, J. Yeo, S. Hong, K. H. Nam, D. Lee, S. S. Lee and S. H. Ko, *Advanced Materials*, 2012, **24**, 3326-3332.
- 15 P. J. Hung, K. Jeong, G. L. Liu and L. P. Lee, *Applied Physics Letters*, 2004, **85**, 6051-6053.
- 16 K. Huang and P. Peumans, *Proc. SPIE-Int. Soc. Opt. Eng*, 2006, **6174**, 617412.
- 17 D.-H. Kim, J. Song, W. M. Choi, H.-S. Kim, R.-H. Kim, Z. Liu, Y. Y. Huang, K.-C. Hwang, Y.-w. Zhang and J. A. Rogers, *Proceedings of the National Academy of Sciences*, 2008, **105**, 18675-18680.
- 18 J. A. Rogers, T. Someya and Y. Huang, *Science*, 2010, **327**, 1603-1607.
- 19 S. P. Lacour, D. Chan, S. Wagner, T. Li and Z. Suo, *Applied Physics Letters*, 2006, **88**, 204103.
- 20 S.-I. Park, J.-H. Ahn, X. Feng, S. Wang, Y. Huang and J. A. Rogers, *Advanced Functional Materials*, 2008, **18**, 2673-2684.
- 21 K. S. Kim, Y. Zhao, H. Jang, S. Y. Lee, J. M. Kim, K. S. Kim, J.-H. Ahn, P. Kim, J.-Y. Choi and B. H. Hong, *Nature*, 2009, **457**, 706-710.
- 22 D.-H. Kim and J. A. Rogers, *Advanced Materials*, 2008, **20**, 4887-4892.
- 23 J. H. Ahn and J. H. Je, *J Phys D Appl Phys*, 2012, **45**, 103001.
- 24 S. M. Bergin, Y.-H. Chen, A. R. Rathmell, P. Charbonneau, Z.-Y. Li and B. J. Wiley, *Nanoscale*, 2012, **4**, 1996-2004.
- 25 B. Vigolo, C. Coulon, M. Maugey, C. Zakri and P. Poulin, *Science*, 2005, **309**, 920-923.
- 26 Y. Xia, P. Yang, Y. Sun, Y. Wu, B. Mayers, B. Gates, Y. Yin, F. Kim and H. Yan, *Advanced Materials*, 2003, **15**, 353-389.
- 27 H.-Y. Shi, B. Hu, X.-C. Yu, R.-L. Zhao, X.-F. Ren, S.-L. Liu, J.-W. Liu, M. Feng, A.-W. Xu and S.-H. Yu, *Advanced Functional Materials*, 2010, **20**, 958-964.
- 28 S. Acharya, A. B. Panda, N. Belman, S. Efrima and Y. Golan, *Advanced Materials*, 2006, **18**, 210-213.
- 29 J.-W. Liu, J.-L. Wang, Z.-H. Wang, W.-R. Huang and S.-H. Yu, *Angewandte Chemie*, 2014, **126**, 13695-13700.
- 30 Y.-T. Tsai, W. Xu, E.-H. Yang and C.-H. Choi, *Nanoscience and Nanotechnology Letters*, 2010, **2**, 150-156.
- 31 Z. Fan, J. C. Ho, Z. A. Jacobson, R. Yerushalmi, R. L. Alley, H. Razavi and A. Javey, *Nano Letters*, 2008, **8**, 20-25.
- 32 R. Yerushalmi, Z. A. Jacobson, J. C. Ho, Z. Fan and A. Javey, *Applied Physics Letters*, 2007, **91**, 203104.
- 33 F. Xu, J. W. Durham, B. J. Wiley and Y. Zhu, *ACS Nano*, 2011, **5**, 1556-1563.
- 34 X. Duan, C. Niu, V. Sahi, J. Chen, J. W. Parce, S. Empedocles and J. L. Goldman, *Nature*, 2003, **425**, 274-278.
- 35 Y. Huang, X. Duan, Q. Wei and C. M. Lieber, *Science*, 2001, **291**, 630-633.
- 36 Y. Li and Y. Wu, *Journal of the American Chemical Society*, 2009, **131**, 5851-5857.
- 37 G. Yu, A. Cao and C. M. Lieber, *Nat Nano*, 2007, **2**, 372-377.
- 38 C. M. Hangarter, Y. Rheem, B. Yoo, E.-H. Yang and N. V. Myung, *Nanotechnology*, 2007, **18**, 205305.
- 39 P. A. Smith, C. D. Nordquist, T. N. Jackson, T. S. Mayer, B. R. Martin, J. Mbindyo and T. E. Mallouk, *Applied Physics Letters*, 2000, **77**, 1399-1401.
- 40 E. M. Freer, O. Grachev, X. Duan, S. Martin and D. P. Stumbo, *Nat Nano*, 2010, **5**, 525-530.
- 41 H. Wu, D. Kong, Z. Ruan, P.-C. Hsu, S. Wang, Z. Yu, T. J. Carney, L. Hu, S. Fan and Y. Cui, *Nat Nano*, 2013, **8**, 421-425.
- 42 A. Pevzner, Y. Engel, R. Elnathan, T. Ducobni, M. Ben-Ishai, K. Reddy, N. Shpaisman, A. Tsukernik, M. Oksman and F. Patolsky, *Nano Letters*, 2010, **10**, 1202-1208.
- 43 V. Scardaci, R. Coull, P. E. Lyons, D. Rickard and J. N. Coleman, *Small*, 2011, **7**, 2621-2628.
- 44 S.-E. Park, S. Kim, D.-Y. Lee, E. Kim and J. Hwang, *Journal of Materials Chemistry A*, 2013, **1**, 14286-14293.
- 45 T. Kim, A. Canlier, G. H. Kim, J. Choi, M. Park and S. M. Han, *ACS Applied Materials & Interfaces*, 2013, **5**, 788-794.
- 46 S. De, T. M. Higgins, P. E. Lyons, E. M. Doherty, P. N. Nirmalraj, W. J. Blau, J. J. Boland and J. N. Coleman, *ACS Nano*, 2009, **3**, 1767-1774.
- 47 L. Hu, H. S. Kim, J.-Y. Lee, P. Peumans and Y. Cui, *ACS Nano*, 2010, **4**, 2955-2963.
- 48 J.-Y. Lee, S. T. Connor, Y. Cui and P. Peumans, *Nano Letters*, 2008, **8**, 689-692.
- 49 J.-Y. Lee, S. T. Connor, Y. Cui and P. Peumans, *Nano Letters*, 2010, **10**, 1276-1279.
- 50 X. Guo, X. Liu, J. Luo, Z. Gan, Z. Meng and N. Zhang, *RSC Advances*, 2015, **5**, 24953-24959.
- 51 M. Song, D. S. You, K. Lim, S. Park, S. Jung, C. S. Kim, D.-H. Kim, D.-G. Kim, J.-K. Kim, J. Park, Y.-C. Kang, J. Heo, S.-H. Jin, J. H. Park and J.-W. Kang, *Advanced Functional Materials*, 2013, **23**, 4177-4184.
- 52 G.-W. Huang, H.-M. Xiao and S.-Y. Fu, *ACS Nano*, 2015, **9**, 3234-3242.
- 53 Y.-M. Chang, W.-Y. Yeh and P.-C. Chen, *Nanotechnology*, 2014, **25**, 285601.
- 54 J. Krantz, M. Richter, S. Spallek, E. Spiecker and C. J. Brabec, *Advanced Functional Materials*, 2011, **21**, 4784-4787.
- 55 J. Ge, H.-B. Yao, X. Wang, Y.-D. Ye, J.-L. Wang, Z.-Y. Wu, J.-W. Liu, F.-J. Fan, H.-L. Gao, C.-L. Zhang and S.-H. Yu, *Angewandte Chemie*, 2013, **125**, 1698-1703.
- 56 Y. Li, P. Cui, L. Wang, H. Lee, K. Lee and H. Lee, *ACS Applied Materials & Interfaces*, 2013, **5**, 9155-9160.

- 57 A. Tao, F. Kim, C. Hess, J. Goldberger, R. He, Y. Sun, Y. Xia and P. Yang, *Nano Letters*, 2003, **3**, 1229-1233.
- 58 P. Yang, *Nature*, 2003, **425**, 243-244.
- 59 J.-W. Liu, J.-L. Wang, Z.-H. Wang, W.-R. Huang and S.-H. Yu, *Angewandte Chemie International Edition*, 2014, **53**, 13477-13482.
- 60 S. Srivastava and N. A. Kotov, *Accounts of Chemical Research*, 2008, **41**, 1831-1841.
- 61 N. Joseph, P. Ahmadiannamini, R. Hoogenboom and I. F. J. Vankelecom, *Polymer Chemistry*, 2014, **5**, 1817-1831.
- 62 F. Xu and Y. Zhu, *Advanced Materials*, 2012, **24**, 5117-5122.
- 63 Y. Cheng, R. Wang, J. Sun and L. Gao, *ACS Nano*, 2015, **9**, 3887-3895.
- 64 R. M. Mutiso, M. C. Sherrott, A. R. Rathmell, B. J. Wiley and K. I. Winey, *ACS Nano*, 2013, **7**, 7654-7663.
- 65 Y. Jin, D. Deng, Y. Cheng, L. Kong and F. Xiao, *Nanoscale*, 2014, **6**, 4812-4818.
- 66 X.-Y. Zeng, Q.-K. Zhang, R.-M. Yu and C.-Z. Lu, *Advanced Materials*, 2010, **22**, 4484-4488.
- 67 L. Yang, T. Zhang, H. Zhou, S. C. Price, B. J. Wiley and W. You, *ACS Applied Materials & Interfaces*, 2011, **3**, 4075-4084.
- 68 H. Guo, N. Lin, Y. Chen, Z. Wang, Q. Xie, T. Zheng, N. Gao, S. Li, J. Kang, D. Cai and D.-L. Peng, *Sci. Rep.*, 2013, **3**.
- 69 Y. Lu, J. Y. Huang, C. Wang, S. Sun and J. Lou, *Nat Nano*, 2010, **5**, 218-224.
- 70 K. Karki, E. Epstein, J.-H. Cho, Z. Jia, T. Li, S. T. Picraux, C. Wang and J. Cumings, *Nano Letters*, 2012, **12**, 1392-1397.
- 71 E. C. Garnett, W. Cai, J. J. Cha, F. Mahmood, S. T. Connor, M. Greyson Christoforo, Y. Cui, M. D. McGehee and M. L. Brongersma, *Nat Mater*, 2012, **11**, 241-249.
- 72 J. Lee, P. Lee, H. Lee, D. Lee, S. S. Lee and S. H. Ko, *Nanoscale*, 2012, **4**, 6408-6414.
- 73 V. C. Tung, L.-M. Chen, M. J. Allen, J. K. Wassei, K. Nelson, R. B. Kaner and Y. Yang, *Nano Letters*, 2009, **9**, 1949-1955.
- 74 A. Malesevic, R. Vitchev, K. Schouteden, A. Volodin, L. Zhang, G. Van Tendeloo, A. Vanhulsel and C. Van Haesendonck, *Nanotechnology*, 2008, **19**, 305604.
- 75 X. Wang, J.-B. Xu, C. Wang, J. Du and W. Xie, *Advanced Materials*, 2011, **23**, 2464-2468.
- 76 J. Park, W. H. Lee, S. Huh, S. H. Sim, S. B. Kim, K. Cho, B. H. Hong and K. S. Kim, *The Journal of Physical Chemistry Letters*, 2011, **2**, 841-845.
- 77 Z. Liu, A. A. Bol and W. Haensch, *Nano Letters*, 2011, **11**, 523-528.
- 78 X. Xie, K. Zhao, X. Xu, W. Zhao, S. Liu, Z. Zhu, M. Li, Z. Shi and Y. Shao, *The Journal of Physical Chemistry C*, 2010, **114**, 14243-14250.
- 79 T. Akter and W. S. Kim, *ACS Applied Materials & Interfaces*, 2012, **4**, 1855-1859.
- 80 M. Göbelt, R. Keding, S. W. Schmitt, B. Hoffmann, S. Jäckle, M. Latzel, V. V. Radmilović, V. R. Radmilović, E. Spiecker and S. Christiansen, *Nano Energy*, 2015, **16**, 196-206.
- 81 R. Zhu, C.-H. Chung, K. C. Cha, W. Yang, Y. B. Zheng, H. Zhou, T.-B. Song, C.-C. Chen, P. S. Weiss, G. Li and Y. Yang, *ACS Nano*, 2011, **5**, 9877-9882.
- 82 S. Choi, J. Park, W. Hyun, J. Kim, J. Kim, Y. B. Lee, C. Song, H. J. Hwang, J. H. Kim, T. Hyeon and D.-H. Kim, *ACS Nano*, 2015, **9**, 6626-6633.
- 83 F. Selzer, Wei, D. Kneppel, L. Bormann, C. Sachse, N. Gaponik, A. Eychmüller, K. Leo and L. Müller-Meskamp, *Nanoscale*, 2015, **7**, 2777-2783.
- 84 W. Gaynor, G. F. Burkhard, M. D. McGehee and P. Peumans, *Advanced Materials*, 2011, **23**, 2905-2910.
- 85 I. K. Moon, J. I. Kim, H. Lee, K. Hur, W. C. Kim and H. Lee, *Sci. Rep.*, 2013, **3**, 112.
- 86 H. Lee, K. Lee, J. T. Park, W. C. Kim and H. Lee, *Advanced Functional Materials*, 2014, **24**, 3276-3283.
- 87 X. Li, F. Zhang and Q. Niu, *Physical Review Letters*, 2013, **110**, 066803.
- 88 H. Castro Neto, F. Guinea, N. M. R. Peres, K. S. Novoselov and A. K. Geim, *Reviews of Modern Physics*, 2009, **81**, 109-162.
- 89 A. K. Geim, *Science*, 2009, **324**, 1530-1534.
- 90 M. I. Katsnelson, K. S. Novoselov and A. K. Geim, *Nat Phys*, 2006, **2**, 620-625.
- 91 J. M. Pereira, V. Milnar, F. M. Peeters and P. Vasilopoulos, *Physical Review B*, 2006, **74**, 045424.
- 92 C. Berger, Z. Song, X. Li, X. Wu, N. Brown, C. Naud, D. Mayou, T. Li, J. Hass, A. N. Marchenkov, E. H. Conrad, P. N. First and W. A. de Heer, *Science*, 2006, **312**, 1191-1196.
- 93 Y. Zhang, Y.-W. Tan, H. L. Stormer and P. Kim, *Nature*, 2005, **438**, 201-204.
- 94 Y. T. Lee, K. Choi, H. S. Lee, S.-W. Min, P. J. Jeon, D. K. Hwang, H. J. Choi and S. Im, *Small*, 2014, **10**, 2356-2361.
- 95 X. Du, I. Skachko, A. Barker and E. Y. Andrei, *Nat Nano*, 2008, **3**, 491-495.
- 96 F. Schedin, A. K. Geim, S. V. Morozov, E. W. Hill, P. Blake, M. I. Katsnelson and K. S. Novoselov, *Nat Mater*, 2007, **6**, 652-655.
- 97 S.-M. Choi, S.-H. Jhi and Y.-W. Son, *Physical Review B*, 2010, **81**, 081407.
- 98 R. Nair, P. Blake, A. N. Grigorenko, K. S. Novoselov, T. J. Booth, T. Stauber, N. M. R. Peres and A. K. Geim, *Science*, 2008, **320**, 1308.
- 99 S. Pang, Y. Hernandez, X. Feng and K. Müllen, *Advanced Materials*, 2011, **23**, 2779-2795.
- 100 G. Eda, G. Fanchini and M. Chhowalla, *Nat Nano*, 2008, **3**, 270-274.
- 101 C. Biswas and Y. H. Lee, *Advanced Functional Materials*, 2011, **21**, 3806-3826.
- 102 C. Mattevi, H. Kim and M. Chhowalla, *Journal of Materials Chemistry*, 2011, **21**, 3324-3334.
- 103 X. Li, Y. Zhu, W. Cai, M. Borysiak, B. Han, D. Chen, R. D. Piner, L. Colombo and R. S. Ruoff, *Nano Letters*, 2009, **9**, 4359-4363.
- 104 J. W. Suk, W. H. Lee, J. Lee, H. Chou, R. D. Piner, Y. Hao, D. Akinwande and R. S. Ruoff, *Nano Letters*, 2013, **13**, 1462-1467.
- 105 Y. Liu, L. Yuan, M. Yang, Y. Zheng, L. Li, L. Gao, N. Nerngchamnon, C. T. Nai, C. S. S. Sangeeth, Y. P. Feng, C. A. Nijhuis and K. P. Loh, *Nat Commun*, 2014, **5**.
- 106 E. H. Lock, M. Baraket, M. Laskoski, S. P. Mulvaney, W. K. Lee, P. E. Sheehan, D. R. Hines, J. T. Robinson, J. Tosado, M. S. Fuhrer, S. C. Hernández and S. G. Walton, *Nano Letters*, 2012, **12**, 102-107.
- 107 T. Yoon, W. C. Shin, T. Y. Kim, J. H. Mun, T.-S. Kim and B. J. Cho, *Nano Letters*, 2012, **12**, 1448-1452.
- 108 S. Bae, H. Kim, Y. Lee, X. Xu, J.-S. Park, Y. Zheng, J. Balakrishnan, T. Lei, H. Ri Kim, Y. I. Song, Y.-J. Kim, K. S. Kim, B. Ozyilmaz, J.-H. Ahn, B. H. Hong and S. Iijima, *Nat Nano*, 2010, **5**, 574-578.
- 109 J. Kang, S. Hwang, J. H. Kim, M. H. Kim, J. Ryu, S. J. Seo, B. H. Hong, M. K. Kim and J.-B. Choi, *ACS Nano*, 2012, **6**, 5360-5365.
- 110 Y. Hernandez, V. Nicolosi, M. Lotya, F. M. Blighe, Z. Sun, S. De, I. T. McGovern, B. Holland, M. Byrne, Y. K. Gun'ko, J. J. Boland, P. Niraj, G. Duesberg, S. Krishnamurthy, R. Goodhue, J. Hutchison, V. Scardaci, A. C. Ferrari and J. N. Coleman, *Nat Nano*, 2008, **3**, 563-568.
- 111 C.-J. Shih, A. Vijayaraghavan, R. Krishnan, R. Sharma, J.-H. Han, M.-H. Ham, Z. Jin, S. Lin, G. L. C. Paulus, N. F. Reuel, Q. H. Wang, D. Blankschtein and M. S. Strano, *Nat Nano*, 2011, **6**, 439-445.
- 112 L. J. Cote, F. Kim and J. Huang, *Journal of the American Chemical Society*, 2009, **131**, 1043-1049.
- 113 S. Gilje, S. Han, M. Wang, K. L. Wang and R. B. Kaner, *Nano Letters*, 2007, **7**, 3394-3398.
- 114 P. Cui, S. Seo, J. Lee, L. Wang, E. Lee, M. Min and H. Lee, *ACS Nano*, 2011, **5**, 6826-6833.

- 115 X. Wang, L. Zhi and K. Müllen, *Nano Letters*, 2008, **8**, 323-327.
- 116 M. Liang, J. Wang, B. Luo, T. Qiu and L. Zhi, *Small*, 2012, **8**, 1180-1184.
- 117 J. Wang, M. Liang, Y. Fang, T. Qiu, J. Zhang and L. Zhi, *Advanced Materials*, 2012, **24**, 2874-2878.
- 118 D. W. Lee, T.-K. Hong, D. Kang, J. Lee, M. Heo, J. Y. Kim, B.-S. Kim and H. S. Shin, *Journal of Materials Chemistry*, 2011, **21**, 3438-3442.
- 119 B. W. An, K. Kim, M. Kim, S.-Y. Kim, S.-H. Hur and J.-U. Park, *Small*, 2015, **11**, 2263-2268.
- 120 D. A. Dikin, S. Stankovich, E. J. Zimney, R. D. Piner, G. H. B. Dommett, G. Evmenenko, S. T. Nguyen and R. S. Ruoff, *Nature*, 2007, **448**, 457-460.
- 121 Y. Yoon, K. Lee, C. Baik, H. Yoo, M. Min, Y. Park, S. M. Lee and H. Lee, *Advanced Materials*, 2013, **25**, 4437-4444.
- 122 S. Seo, M. Min, J. Lee, T. Lee, S.-Y. Choi and H. Lee, *Angewandte Chemie International Edition*, 2012, **51**, 108-112.
- 123 M. Min, S. Seo, S. M. Lee and H. Lee, *Advanced Materials*, 2013, **25**, 7045-7050.
- 124 N. Behabtu, J. R. Lomeda, M. J. Green, A. L. Higginbotham, A. Sinititskii, D. V. Kosynkin, D. Tsentlovich, A. N. G. Parra-Vasquez, J. Schmidt, E. Kesselman, Y. Cohen, Y. Talmon, J. M. Tour and M. Pasquali, *Nat Nano*, 2010, **5**, 406-411.
- 125 B. G. Choi, H. Park, T. J. Park, M. H. Yang, J. S. Kim, S.-Y. Jang, N. S. Heo, S. Y. Lee, J. Kong and W. H. Hong, *ACS Nano*, 2010, **4**, 2910-2918.
- 126 L. Gao, W. Ren, H. Xu, L. Jin, Z. Wang, T. Ma, L.-P. Ma, Z. Zhang, Q. Fu, L.-M. Peng, X. Bao and H.-M. Cheng, *Nat Commun*, 2012, **3**, 699.
- 127 Z. Li, P. Wu, C. Wang, X. Fan, W. Zhang, X. Zhai, C. Zeng, Z. Li, J. Yang and J. Hou, *ACS Nano*, 2011, **5**, 3385-3390.
- 128 X. Li, C. W. Magnuson, A. Venugopal, J. An, J. W. Suk, B. Han, M. Borysiak, W. Cai, A. Velamakanni, Y. Zhu, L. Fu, E. M. Vogel, E. Voelkl, L. Colombo and R. S. Ruoff, *Nano Letters*, 2010, **10**, 4328-4334.
- 129 I. Vlassiouk, M. Regmi, P. Fulvio, S. Dai, P. Datskos, G. Eres and S. Smirnov, *ACS Nano*, 2011, **5**, 6069-6076.
- 130 X. Dong, D. Fu, W. Fang, Y. Shi, P. Chen and L.-J. Li, *Small*, 2009, **5**, 1422-1426.
- 131 H. Wang, T. Maiyalagan and X. Wang, *ACS Catalysis*, 2012, **2**, 781-794.
- 132 L. G. Cançado, A. Jorio, E. H. M. Ferreira, F. Stavale, C. A. Achete, R. B. Capaz, M. V. O. Moutinho, A. Lombardo, T. S. Kulmala and A. C. Ferrari, *Nano Letters*, 2011, **11**, 3190-3196.
- 133 V. Singh, D. Joung, L. Zhai, S. Das, S. I. Khondaker and S. Seal, *Progress in Materials Science*, 2011, **56**, 1178-1271.
- 134 V. López, R. S. Sundaram, C. Gómez-Navarro, D. Olea, M. Burghard, J. Gómez-Herrero, F. Zamora and K. Kern, *Advanced Materials*, 2009, **21**, 4683-4686.
- 135 S. Stankovich, D. A. Dikin, R. D. Piner, K. A. Kohlhaas, A. Kleinhammes, Y. Jia, Y. Wu, S. T. Nguyen and R. S. Ruoff, *Carbon*, 2007, **45**, 1558-1565.
- 136 G. Eda and M. Chhowalla, *Advanced Materials*, 2010, **22**, 2392-2415.
- 137 S. Stankovich, D. A. Dikin, G. H. B. Dommett, K. M. Kohlhaas, E. J. Zimney, E. A. Stach, R. D. Piner, S. T. Nguyen and R. S. Ruoff, *Nature*, 2006, **442**, 282-286.
- 138 Y. Si and E. T. Samulski, *Nano Letters*, 2008, **8**, 1679-1682.
- 139 C. Chen, T. Chen, H. Wang, G. Sun and X. Yang, *Nanotechnology*, 2011, **22**, 405602.
- 140 A. B. Bourlinos, D. Gournis, D. Petridis, T. Szabó, A. Szeri and I. Dékány, *Langmuir*, 2003, **19**, 6050-6055.
- 141 Y. Chen, X. Zhang, P. Yu and Y. Ma, *Chemical Communications*, 2009, 4527-4529.
- 142 D. Yang, A. Velamakanni, G. Bozoklu, S. Park, M. Stoller, R. D. Piner, S. Stankovich, I. Jung, D. A. Field, C. A. Ventrice Jr and R. S. Ruoff, *Carbon*, 2009, **47**, 145-152.
- 143 Y. Yoon, S. Seo, G. Kim and H. Lee, *Chemistry – A European Journal*, 2012, **18**, 13466-13472.
- 144 A. Bagri, C. Mattevi, M. Acik, Y. J. Chabal, M. Chhowalla and V. B. Shenoy, *Nat Chem*, 2010, **2**, 581-587.
- 145 F.-A. He, J.-T. Fan, F. Song, L.-M. Zhang and H. Lai-Wa Chan, *Nanoscale*, 2011, **3**, 1182-1188.
- 146 C. Hamilton, J. Lomeda, Z. Sun, J. Tour and A. Barron, *Nano Res.*, 2010, **3**, 138-145.
- 147 Z. Yang, Y. Sun, L. B. Alemany, T. N. Narayanan and W. E. Billups, *Journal of the American Chemical Society*, 2012, **134**, 18689-18694.
- 148 X. Zhong, J. Jin, S. Li, Z. Niu, W. Hu, R. Li and J. Ma, *Chemical Communications*, 2010, **46**, 7340-7342.
- 149 J. Choi, K.-j. Kim, B. Kim, H. Lee and S. Kim, *The Journal of Physical Chemistry C*, 2009, **113**, 9433-9435.
- 150 S. Sarkar, E. Bekyarova, S. Niyogi and R. C. Haddon, *Journal of the American Chemical Society*, 2011, **133**, 3324-3327.
- 151 J. R. Lomeda, C. D. Doyle, D. V. Kosynkin, W.-F. Hwang and J. M. Tour, *Journal of the American Chemical Society*, 2008, **130**, 16201-16206.
- 152 H. Liu, S. Ryu, Z. Chen, M. L. Steigerwald, C. Nuckolls and L. E. Brus, *Journal of the American Chemical Society*, 2009, **131**, 17099-17101.
- 153 H. Li, T. Lu, L. Pan, Y. Zhang and Z. Sun, *Journal of Materials Chemistry*, 2009, **19**, 6773-6779.
- 154 J. W. Colson, A. R. Woll, A. Mukherjee, M. P. Levendorf, E. L. Spitzer, V. B. Shields, M. G. Spencer, J. Park and W. R. Dichtel, *Science*, 2011, **332**, 228-231.
- 155 J. M. MacLeod and F. Rosei, *Small*, 2014, **10**, 1038-1049.
- 156 Y. Wang, X. Chen, Y. Zhong, F. Zhu and K. P. Loh, *Applied Physics Letters*, 2009, **95**, 063302.
- 157 E.-Y. Choi, T. H. Han, J. Hong, J. E. Kim, S. H. Lee, H. W. Kim and S. O. Kim, *Journal of Materials Chemistry*, 2010, **20**, 1907-1912.
- 158 Y.-L. Li, C.-F. Kuan, C.-H. Chen, H.-C. Kuan, M.-C. Yip, S.-L. Chiu and C.-L. Chiang, *Materials Chemistry and Physics*, 2012, **134**, 677-685.
- 159 A. Zintchenko, A. Philipp, A. Dehshahri and E. Wagner, *Bioconjugate Chemistry*, 2008, **19**, 1448-1455.
- 160 Y. Zhu, Q. Qin, F. Xu, F. Fan, Y. Ding, T. Zhang, B. J. Wiley and Z. L. Wang, *Physical Review B*, 2012, **85**, 045443.
- 161 S. Vlassov, B. Polyakov, L. M. Dorogin, M. Antsov, M. Mets, M. Umalas, R. Saar, R. Löhmus and I. Kink, *Materials Chemistry and Physics*, 2014, **143**, 1026-1031.
- 162 S. Sorel, P. E. Lyons, S. De, J. C. Dickerson and J. N. Coleman, *Nanotechnology*, 2012, **23**, 185201.
- 163 K. L. Lin, J. Chae and K. Jain, *Advanced Packaging, IEEE Transactions on*, 2010, **33**, 592-601.
- 164 H. Lee, G. Han, M. Kim, H.-s. Ahn and H. Lee, *Advanced Materials*, 2015, **27**, 2252-2259.
- 165 C. Lee, X. Wei, J. W. Kysar and J. Hone, *Science*, 2008, **321**, 385-388.
- 166 H. Zhao and N. R. Aluru, *Journal of Applied Physics*, 2010, **108**, 064321.
- 167 D. L. Duong, G. H. Han, S. M. Lee, F. Gunes, E. S. Kim, S. T. Kim, H. Kim, Q. H. Ta, K. P. So, S. J. Yoon, S. J. Chae, Y. W. Jo, M. H. Park, S. H. Chae, S. C. Lim, J. Y. Choi and Y. H. Lee, *Nature*, 2012, **490**, 235-239.
- 168 M.-F. Yu, O. Lourie, M. J. Dyer, K. Moloni, T. F. Kelly and R. S. Ruoff, *Science*, 2000, **287**, 637-640.
- 169 J. Zang, S. Ryu, N. Pugno, Q. Wang, Q. Tu, M. J. Buehler and X. Zhao, *Nat Mater*, 2013, **12**, 321-325.
- 170 T. Chen, Y. Xue, A. K. Roy and L. Dai, *ACS Nano*, 2014, **8**, 1039-1046.
- 171 Z. Chen, W. Ren, L. Gao, B. Liu, S. Pei and H.-M. Cheng, *Nat Mater*, 2011, **10**, 424-428.

- 172 P. Lee, J. Ham, J. Lee, S. Hong, S. Han, Y. D. Suh, S. E. Lee, J. Yeo, S. S. Lee, D. Lee and S. H. Ko, *Advanced Functional Materials*, 2014, **24**, 5671-5678.
- 173 K. Zhang, L. L. Zhang, X. S. Zhao and J. Wu, *Chemistry of Materials*, 2010, **22**, 1392-1401.
- 174 L. L. Zhang, S. Zhao, X. N. Tian and X. S. Zhao, *Langmuir*, 2010, **26**, 17624-17628.
- 175 Q. Liu, Z. Liu, X. Zhang, L. Yang, N. Zhang, G. Pan, S. Yin, Y. Chen and J. Wei, *Advanced Functional Materials*, 2009, **19**, 894-904.
- 176 S. Huang, L. Ren, J. Guo, H. Zhu, C. Zhang and T. Liu, *Carbon*, 2012, **50**, 216-224.
- 177 L. Mao, Y. Li, C. Chi, H. S. On Chan and J. Wu, *Nano Energy*, 2014, **6**, 119-128.
- 178 T. Tokuno, M. Nogi, J. Jiu and K. Suganuma, *Nanoscale Res Lett*, 2012, **7**, 1-7.
- 179 J. O. Hwang, J. S. Park, D. S. Choi, J. Y. Kim, S. H. Lee, K. E. Lee, Y.-H. Kim, M. H. Song, S. Yoo and S. O. Kim, *ACS Nano*, 2012, **6**, 159-167.
- 180 P. V. Kumar, M. Bernardi and J. C. Grossman, *ACS Nano*, 2013, **7**, 1638-1645.
- 181 B. Kang, S. Lim, W. H. Lee, S. B. Jo and K. Cho, *Advanced Materials*, 2013, **25**, 5856-5862.
- 182 Y. Shi, K. K. Kim, A. Reina, M. Hofmann, L.-J. Li and J. Kong, *ACS Nano*, 2010, **4**, 2689-2694.
- 183 T. H. Seo, S. J. Chae, B. K. Kim, G. Shin, Y. H. Lee and E.-K. Suh, *Applied Physics Express*, 2012, **5**, 115101.
- 184 R. Chen, S. R. Das, C. Jeong, M. R. Khan, D. B. Janes and M. A. Alam, *Advanced Functional Materials*, 2013, **23**, 5150-5158.
- 185 C. Wu, L. Fang, X. Huang and P. Jiang, *ACS Applied Materials & Interfaces*, 2014, **6**, 21026-21034.
- 186 B. W. An, B. G. Hyun, S.-Y. Kim, M. Kim, M.-S. Lee, K. Lee, J. B. Koo, H. Y. Chu, B.-S. Bae and J.-U. Park, *Nano Letters*, 2014, **14**, 6322-6328.
- 187 J. Wu, M. Agrawal, H. A. Becerril, Z. Bao, Z. Liu, Y. Chen and P. Peumans, *ACS Nano*, 2010, **4**, 43-48.
- 188 K.-H. Ok, J. Kim, S.-R. Park, Y. Kim, C.-J. Lee, S.-J. Hong, M.-G. Kwak, N. Kim, C. J. Han and J.-W. Kim, *Sci. Rep.*, 2015, **5**.
- 189 J. Liang, L. Li, X. Niu, Z. Yu and Q. Pei, *Nat Photon*, 2013, **7**, 817-824.
- 190 J. Liang, L. Li, K. Tong, Z. Ren, W. Hu, X. Niu, Y. Chen and Q. Pei, *ACS Nano*, 2014, **8**, 1590-1600.
- 191 T.-H. Han, Y. Lee, M.-R. Choi, S.-H. Woo, S.-H. Bae, B. H. Hong, J.-H. Ahn and T.-W. Lee, *Nat Photon*, 2012, **6**, 105-110.
- 192 F. Withers, O. Del Pozo-Zamudio, A. Mishchenko, A. P. Rooney, A. Gholinia, K. Watanabe, T. Taniguchi, S. J. Haigh, A. K. Geim, A. I. Tartakovskii and K. S. Novoselov, *Nat Mater*, 2015, **14**, 301-306.
- 193 F. C. Krebs, *Solar Energy Materials and Solar Cells*, 2009, **93**, 1636-1641.
- 194 Y. Kim, T. I. Ryu, K.-H. Ok, M.-G. Kwak, S. Park, N.-G. Park, C. J. Han, B. S. Kim, M. J. Ko, H. J. Son and J.-W. Kim, *Advanced Functional Materials*, 2015, n/a-n/a.
- 195 Y. Jin, L. Li, Y. Cheng, L. Kong, Q. Pei and F. Xiao, *Advanced Functional Materials*, 2015, **25**, 1581-1587.
- 196 M. Cox, A. Gorodetsky, B. Kim, K. S. Kim, Z. Jia, P. Kim, C. Nuckolls and I. Kymissis, *Applied Physics Letters*, 2011, **98**, 123303.
- 197 Y. Wang, S. W. Tong, X. F. Xu, B. Özyilmaz and K. P. Loh, *Advanced Materials*, 2011, **23**, 1514-1518.
- 198 A. Matković, U. Ralević, G. Isić, M. M. Jakovljević, B. Vasić, I. Milošević, D. Marković and R. Gajić, *Physica Scripta*, 2012, 014069.
- 199 H. Tong-Hun, C. Wen-Hai, Y. Ik-Seok and K. Oh-Kyong, *Consumer Electronics, IEEE Transactions on*, 2010, **56**, 1115-1122.
- 200 J. Lee, P. Lee, H. B. Lee, S. Hong, I. Lee, J. Yeo, S. S. Lee, T.-S. Kim, D. Lee and S. H. Ko, *Advanced Functional Materials*, 2013, **23**, 4171-4176.
- 201 E. O. Polat, O. Balci and C. Kocabas, *Sci. Rep.*, 2014, **4**.
- 202 C. R. Siju, L. Raja, N. C. Shivaprakash and S. Sindhu, *J Solid State Electrochem*, 2015, **19**, 1393-1402.
- 203 C. Yan, W. Kang, J. Wang, M. Cui, X. Wang, C. Y. Foo, K. J. Chee and P. S. Lee, *ACS Nano*, 2014, **8**, 316-322.
- 204 S. Seo, M. Min, S. M. Lee and H. Lee, *Nat Commun*, 2013, **4**, 1920.
- 205 P. Yao, P. Chen, L. Jiang, H. Zhao, H. Zhu, D. Zhou, W. Hu, B.-H. Han and M. Liu, *Advanced Materials*, 2010, **22**, 5008-5012.
- 206 J. Wang, C. Yan, W. Kang and P. S. Lee, *Nanoscale*, 2014, **6**, 10734-10739.
- 207 J. Liu, T.-M. Fu, Z. Cheng, G. Hong, T. Zhou, L. Jin, M. Duvvuri, Z. Jiang, P. Kruskal, C. Xie, Z. Suo, Y. Fang and C. M. Lieber, *Nat Nano*, 2015, **10**, 629-636.
- 208 Z. Liu, J. T. Robinson, X. Sun and H. Dai, *Journal of the American Chemical Society*, 2008, **130**, 10876-10877.
- 209 N. Mohanty and V. Berry, *Nano Letters*, 2008, **8**, 4469-4476.
- 210 J.-F. Wu, M.-Q. Xu and G.-C. Zhao, *Electrochemistry Communications*, 2010, **12**, 175-177.
- 211 M. Luo, X. Chen, G. Zhou, X. Xiang, L. Chen, X. Ji and Z. He, *Chemical Communications*, 2012, **48**, 1126-1128.
- 212 W. Gao, Y. Chen, J. Xi, S. Lin, Y. Chen, Y. Lin and Z. Chen, *Biosensors and Bioelectronics*, 2013, **41**, 776-782.
- 213 T. Liu, H. Su, X. Qu, P. Ju, L. Cui and S. Ai, *Sensors and Actuators B: Chemical*, 2011, **160**, 1255-1261.
- 214 W. Song, D.-W. Li, Y.-T. Li, Y. Li and Y.-T. Long, *Biosensors and Bioelectronics*, 2011, **26**, 3181-3186.
- 215 X. Kang, J. Wang, H. Wu, I. A. Aksay, J. Liu and Y. Lin, *Biosensors and Bioelectronics*, 2009, **25**, 901-905.
- 216 L. Wang, X. Zhang, H. Xiong and S. Wang, *Biosensors and Bioelectronics*, 2010, **26**, 991-995.
- 217 M. Zhang, C. Liao, Y. Yao, Z. Liu, F. Gong and F. Yan, *Advanced Functional Materials*, 2014, **24**, 978-985.
- 218 X. Yang, J. Bai, Y. Wang, X. Jiang and X. He, *Analyst*, 2012, **137**, 4362-4367.
- 219 V. Benfenati, S. Toffanin, S. Bonetti, G. Turatti, A. Pistone, M. Chiappalone, A. Sagnella, A. Stefani, G. Generali, G. Ruani, D. Saguatti, R. Zamboni and M. Muccini, *Nat Mater*, 2013, **12**, 672-680.
- 220 D.-H. Kim, N. Lu, R. Ghaffari, Y.-S. Kim, S. P. Lee, L. Xu, J. Wu, R.-H. Kim, J. Song, Z. Liu, J. Vimenti, B. de Graff, B. Elolampi, M. Mansour, M. J. Slepian, S. Hwang, J. D. Moss, S.-M. Won, Y. Huang, B. Litt and J. A. Rogers, *Nat Mater*, 2011, **10**, 316-323.
- 221 M. Berggren and A. Richter-Dahlfors, *Advanced Materials*, 2007, **19**, 3201-3213.
- 222 T. Cohen-Karni, Q. Qing, Q. Li, Y. Fang and C. M. Lieber, *Nano Letters*, 2010, **10**, 1098-1102.
- 223 D.-W. Park, A. A. Schendel, S. Mikael, S. K. Brodnick, T. J. Richner, J. P. Ness, M. R. Hayat, F. Atry, S. T. Frye, R. Pashaie, S. Thongpang, Z. Ma and J. C. Williams, *Nat Commun*, 2014, **5**.
- 224 S. Yun, X. Niu, Z. Yu, W. Hu, P. Brochu and Q. Pei, *Advanced Materials*, 2012, **24**, 1321-1327.
- 225 J. Wu, J. Zang, A. R. Rathmell, X. Zhao and B. J. Wiley, *Nano Letters*, 2013, **13**, 2381-2386.
- 226 J. Liang, Y. Huang, J. Oh, M. Kozlov, D. Sui, S. Fang, R. H. Baughman, Y. Ma and Y. Chen, *Advanced Functional Materials*, 2011, **21**, 3778-3784.
- 227 Y. Tang, S. Gong, Y. Chen, L. W. Yap and W. Cheng, *ACS Nano*, 2014, **8**, 5707-5714.
- 228 J. Wang, J. Jiu, M. Nogi, T. Sugahara, S. Nagao, H. Koga, P. He and K. Suganuma, *Nanoscale*, 2015, **7**, 2926-2932.
- 229 Y. R. Jeong, H. Park, S. W. Jin, S. Y. Hong, S.-S. Lee and J. S. Ha, *Advanced Functional Materials*, 2015, **25**, 4228-4236.
- 230 B. C. K. Tee, C. Wang, R. Allen and Z. Bao, *Nat Nano*, 2012, **7**, 825-832.

- 231 C. Hou, T. Huang, H. Wang, H. Yu, Q. Zhang and Y. Li, *Sci. Rep.*, 2013, **3**.
- 232 V. H. Luan, H. N. Tien, T. V. Cuong, B.-S. Kong, J. S. Chung, E. J. Kim and S. H. Hur, *Journal of Materials Chemistry*, 2012, **22**, 8649-8653.
- 233 T. Ando, *NPG Asia Mater*, 2009, **1**, 17-21.
- 234 K. C. Kwon, K. S. Choi and S. Y. Kim, *Advanced Functional Materials*, 2012, **22**, 4724-4731.
- 235 K. C. Kwon, B. J. Kim, J.-L. Lee and S. Y. Kim, *Journal of Materials Chemistry C*, 2013, **1**, 2463-2469.
- 236 K. C. Kwon, K. S. Choi, C. Kim and S. Y. Kim, *The Journal of Physical Chemistry C*, 2014, **118**, 8187-8193.
- 237 S. Tongay, K. Berke, M. Lemaitre, Z. Nasrollahi, D. B. Tanner, A. F. Hebard and B. R. Appleton, *Nanotechnology*, 2011, **22**.
- 238 H. Pinto, R. Jones, J. P. Goss and P. R. Briddon, *J Phys-Condens Mat*, 2009, **21**.
- 239 C.-L. Hsu, C.-T. Lin, J.-H. Huang, C.-W. Chu, K.-H. Wei and L.-J. Li, *ACS Nano*, 2012, **6**, 5031-5039.
- 240 Q. Su, S. Pang, V. Aljani, C. Li, X. Feng and K. Müllen, *Advanced Materials*, 2009, **21**, 3191-3195.
- 241 M. C. Prado, R. Nascimento, L. G. Moura, M. J. S. Matos, M. S. C. Mazzoni, L. G. Cancado, H. Chacham and B. R. A. Neves, *ACS Nano*, 2011, **5**, 394-398.
- 242 B. Lee, Y. Chen, F. Duerr, D. Mastrogiovanni, E. Garfunkel, E. Y. Andrei and V. Podzorov, *Nano Letters*, 2010, **10**, 2427-2432.
- 243 B. Das, R. Voggu, C. S. Rout and C. N. R. Rao, *Chemical Communications*, 2008, 5155-5157.
- 244 P. Wei, N. Liu, H. R. Lee, E. Adijanto, L. Ci, B. D. Naab, J. Q. Zhong, J. Park, W. Chen, Y. Cui and Z. Bao, *Nano Letters*, 2013, **13**, 1890-1897.
- 245 J. B. Bult, R. Crisp, C. L. Perkins and J. L. Blackburn, *ACS Nano*, 2013, **7**, 7251-7261.
- 246 V. Rakesh, D. Barun, R. Chandra Sekhar and C. N. R. Rao, *Journal of Physics: Condensed Matter*, 2008, **20**, 472204.
- 247 C.-H. Chang, X. Fan, L.-J. Li and J.-L. Kuo, *The Journal of Physical Chemistry C*, 2012, **116**, 13788-13794.
- 248 X. Wang, J.-B. Xu, W. Xie and J. Du, *The Journal of Physical Chemistry C*, 2011, **115**, 7596-7602.
- 249 H. Huang, S. Chen, X. Gao, W. Chen and A. T. S. Wee, *ACS Nano*, 2009, **3**, 3431-3436.
- 250 W. Hong, Y. Xu, G. Lu, C. Li and G. Shi, *Electrochemistry Communications*, 2008, **10**, 1555-1558.
- 251 L. Yangqiao, G. Lian, S. Jing, W. Yan and Z. Jing, *Nanotechnology*, 2009, **20**, 465605.
- 252 H. Wang, Q. Hao, X. Yang, L. Lu and X. Wang, *Electrochemistry Communications*, 2009, **11**, 1158-1161.
- 253 S. Wang, D. Yu, L. Dai, D. W. Chang and J.-B. Baek, *ACS Nano*, 2011, **5**, 6202-6209.
- 254 L. M. Veca, F. Lu, M. J. Meziani, L. Cao, P. Zhang, G. Qi, L. Qu, M. Shrestha and Y.-P. Sun, *Chemical Communications*, 2009, 2565-2567.
- 255 Z. Liu, Q. Liu, Y. Huang, Y. Ma, S. Yin, X. Zhang, W. Sun and Y. Chen, *Advanced Materials*, 2008, **20**, 3924-3930.
- 256 N. A. Kumar, H.-J. Choi, Y. R. Shin, D. W. Chang, L. Dai and J.-B. Baek, *ACS Nano*, 2012, **6**, 1715-1723.
- 257 S. Wang, P.-J. Chia, L.-L. Chua, L.-H. Zhao, R.-Q. Png, S. Sivaramakrishnan, M. Zhou, R. G. S. Goh, R. H. Friend, A. T. S. Wee and P. K. H. Ho, *Advanced Materials*, 2008, **20**, 3440-3446.
- 258 S. Niyogi, E. Bekyarova, M. E. Itkis, J. L. McWilliams, M. A. Hamon and R. C. Haddon, *Journal of the American Chemical Society*, 2006, **128**, 7720-7721.
- 259 S. Stankovich, R. D. Piner, S. T. Nguyen and R. S. Ruoff, *Carbon*, 2006, **44**, 3342-3347.
- 260 N. Karousis, S. P. Economopoulos, E. Sarantopoulou and N. Tagmatarchis, *Carbon*, 2010, **48**, 854-860.
- 261 Y. Xu, Z. Liu, X. Zhang, Y. Wang, J. Tian, Y. Huang, Y. Ma, X. Zhang and Y. Chen, *Advanced Materials*, 2009, **21**, 1275-1279.
- 262 Z.-B. Liu, Y.-F. Xu, X.-Y. Zhang, X.-L. Zhang, Y.-S. Chen and J.-G. Tian, *The Journal of Physical Chemistry B*, 2009, **113**, 9681-9686.
- 263 X. Sun, Z. Liu, K. Welscher, J. Robinson, A. Goodwin, S. Zaric and H. Dai, *Nano Res.*, 2008, **1**, 203-212.
- 264 H. Bao, Y. Pan, Y. Ping, N. G. Sahoo, T. Wu, L. Li, J. Li and L. H. Gan, *Small*, 2011, **7**, 1569-1578.
- 265 B. Chen, M. Liu, L. Zhang, J. Huang, J. Yao and Z. Zhang, *Journal of Materials Chemistry*, 2011, **21**, 7736-7741.
- 266 X. Yang, X. Zhang, Z. Liu, Y. Ma, Y. Huang and Y. Chen, *The Journal of Physical Chemistry C*, 2008, **112**, 17554-17558.
- 267 H. Yang, C. Shan, F. Li, D. Han, Q. Zhang and L. Niu, *Chemical Communications*, 2009, 3880-3882.
- 268 H. Yang, F. Li, C. Shan, D. Han, Q. Zhang, L. Niu and A. Ivaska, *Journal of Materials Chemistry*, 2009, **19**, 4632-4638.
- 269 S. Sarkar, S. Niyogi, E. Bekyarova and R. C. Haddon, *Chemical Science*, 2011, **2**, 1326-1333.
- 270 S. Yang, L. Zhi, K. Tang, X. Feng, J. Maier and K. Müllen, *Advanced Functional Materials*, 2012, **22**, 3634-3640.
- 271 Z.-H. Sheng, H.-L. Gao, W.-J. Bao, F.-B. Wang and X.-H. Xia, *Journal of Materials Chemistry*, 2012, **22**, 390-395.
- 272 W. H. Lee, J. W. Suk, H. Chou, J. Lee, Y. Hao, Y. Wu, R. Piner, D. Akinwande, K. S. Kim and R. S. Ruoff, *Nano Letters*, 2012, **12**, 2374-2378.
- 273 C. K. Chua, A. Ambrosi and M. Pumera, *Chemical Communications*, 2012, **48**, 5376-5378.
- 274 I. N. Kholmanov, S. H. Domingues, H. Chou, X. Wang, C. Tan, J.-Y. Kim, H. Li, R. Piner, A. J. G. Zarbin and R. S. Ruoff, *ACS Nano*, 2013, **7**, 1811-1816.
- 275 *Nanoscale*, 2015, **7**, 6798.
- 276 P. Lee, J. Ham, J. Lee, S. Hong, S. Han, Y. D. Suh, S. E. Lee, J. Yeo, S. S. Lee, D. Lee and S. H. Ko, *Advanced Functional Materials*, 2014, **24**, 5671-5678.
- 277 Y. Ahn, Y. Jeong and Y. Lee, *ACS Applied Materials & Interfaces*, 2012, **4**, 6410-6414.
- 278 J. Kim, M.-S. Lee, S. Jeon, M. Kim, S. Kim, F. Bien, S. Y. Hong and J.-U. Park, *Advanced Materials*, 2015, **27**, 3292-3297.
- 279 J. Zhao, S. Pei, W. Ren, L. Gao and H.-M. Cheng, *ACS Nano*, 2010, **4**, 5245-5252.
- 280 D. Konios, C. Petridis, G. Kakavelakis, M. Sygletou, K. Savva, E. Stratakis and E. Kymakis, *Advanced Functional Materials*, 2015, **25**, 2213-2221.
- 281 H. A. Becerril, J. Mao, Z. Liu, R. M. Stoltenberg, Z. Bao and Y. Chen, *ACS Nano*, 2008, **2**, 463-470.
- 282 J. Chen, H. Bi, S. Sun, Y. Tang, W. Zhao, T. Lin, D. Wan, F. Huang, X. Zhou, X. Xie and M. Jiang, *ACS Applied Materials & Interfaces*, 2013, **5**, 1408-1413.
- 283 H.-J. Shin, K. K. Kim, A. Benayad, S.-M. Yoon, H. K. Park, I.-S. Jung, M. H. Jin, H.-K. Jeong, J. M. Kim, J.-Y. Choi and Y. H. Lee, *Advanced Functional Materials*, 2009, **19**, 1987-1992.
- 284 J. Wu, H. A. Becerril, Z. Bao, Z. Liu, Y. Chen and P. Peumans, *Applied Physics Letters*, 2008, **92**, 263302.
- 285 J. Ning, D. Wang, C. Zhang, Z. Wang, S. Tang, D. Chen, Y. Shi, J. Zhang and Y. Hao, *Synthetic Metals*, 2015, **203**, 215-220.
- 286 M. S. White, M. Kaltenbrunner, E. D. Glowacki, K. Gutnichenko, G. Kettlgruber, I. Graz, S. Aazou, C. Ulbricht, D. A. M. Egbe, M. C. Miron, Z. Major, M. C. Scharber, T. Sekitani, T. Someya, S. Bauer and N. S. Sariciftci, *Nat Photon*, 2013, **7**, 811-816.
- 287 X. Qi, C. Tan, J. Wei and H. Zhang, *Nanoscale*, 2013, **5**, 1440-1451.
- 288 Y. Ahn, Y. Jeong, D. Lee and Y. Lee, *ACS Nano*, 2015, **9**, 3125-3133.
- 289 I. N. Kholmanov, C. W. Magnuson, A. E. Aliev, H. Li, B. Zhang, J. W. Suk, L. L. Zhang, E. Peng, S. H. Mousavi, A. B. Khanikaev, R. Piner, G. Shvets and R. S. Ruoff, *Nano Letters*, 2012, **12**, 5679-5683.

- 290 M.-S. Lee, K. Lee, S.-Y. Kim, H. Lee, J. Park, K.-H. Choi, H.-K. Kim, D.-G. Kim, D.-Y. Lee, S. Nam and J.-U. Park, *Nano Letters*, 2013, **13**, 2814-2821.
- 291 K. Kim, J. Kim, B. G. Hyun, S. Ji, S.-Y. Kim, S. Kim, B. W. An and J.-U. Park, *Nanoscale*, 2015, **7**, 14577-14594.
- 292 T. Cheng, Y. Zhang, W.-Y. Lai and W. Huang, *Advanced Materials*, 2015, **27**, 3349-3376.
- 293 N. Lu, Z. Suo, J. J. Vlassak, *Acta Materialia* 2010, **58**, 1679
- 294 A. R. Rathmell, M. Nguyen, M. Chi and B. J. Wiley, *Nano Letters*, 2012, **12**, 3193-3199.
- 295 A. R. Rathmell and B. J. Wiley, *Advanced Materials*, 2011, **23**, 4798-4803.
- 296 D. Zhang, R. Wang, M. Wen, D. Weng, X. Cui, J. Sun, H. Li and Y. Lu, *Journal of the American Chemical Society*, 2012, **134**, 14283-14286.
- 297 Q. Zhang, Y. A. N. Li, D. Xu and Z. Gu, *Journal of Materials Science Letters*, 2001, **20**, 925-927.
- 298 Xia, Y., Yang, P., Sun, Y., Wu, Y., Mayers, B., Gates, B., and Yan, H, *Advanced materials*, 2003, **15**(5), 353-389
- 299 Y. Zhang, J. Liu, R. He, Q. Zhang, X. Zhang and J. Zhu, *Chemical Physics Letters*, 2002, **360**, 579-584.
- 300 J. U. Kim, S. H. Cha, K. Shin, J. Y. Jho and J. C. Lee, *Advanced Materials*, 2004, **16**, 459-464.
- 301 J. Richter, M. Mertig, W. Pompe, I. Mönch and H. K. Schackert, *Applied Physics Letters*, 2001, **78**, 536-538.
- 302 B. H. Hong, S. C. Bae, C.-W. Lee, S. Jeong and K. S. Kim, *Science*, 2001, **294**, 348-351.
- 303 J. M. Englert, K. C. Knirsch, C. Dotzer, B. Butz, F. Hauke, E. Spiecker and A. Hirsch, *Chemical Communications*, 2012, **48**, 5025-5027.
- 304 S. H. Varela-Rizo, I. Martín-Gullón and M. Terrones, *ACS Nano*, 2012, **6**, 4565-4572.